ISSN 2409-5613 (print)
ISSN 2411-1414 (online)

Chimica Techno Acta

2020. Vol. 7. N 3

cta.urfu.ru

Chimica Techno Acta

2020 | Vol. 7 | No. 3

Scientific and Technical Journal
Established in 2014
Published four times per year

Founded by Ural Federal University named after the first President of Russia B. N. Yeltsin
19, Mira St., Ekaterinburg, 620002, Russia

Chimica Techno Acta

2020 | Vol. 7 | № 3

Научно-технический журнал
Журнал основан в 2014 г.
Выходит четыре раза в год

Учредитель — Уральский федеральный университет имени первого Президента России Б. Н. Ельцина
620002, Россия, Екатеринбург, ул. Мира, 19

Graphical Abstracts

CONTENTS/СОДЕРЖАНИЕ

Chimica Techno Acta
2020. Vol. 7, no. 3

Chimica Techno Acta. 2020. Vol. 7, no. 3. P. 96–103.
ISSN 2409–5613

DOI: 10.15826/chimtech.2020.7.3.01

**Emiliya V. Nosova,[ab*] Olga A. Batanova,[a]
Nataliya N. Mochulskaya,[a] Galina N. Lipunova[b]**

[a] *Ural Federal University*
620002, 19 Mira St., Ekaterinburg, Russia
[b] *I. Ya. Postovskii Institute of Organic Synthesis,*
Ural Branch of Russian Academy of Sciences,
620990, 22 Kovalevskaya St. / 20 Akademicheskaya St., Ekaterinburg, Russia
**email: emilia.nosova@yandex.ru*

Synthetic approaches to 2-aryl/hetaryl- and 2-(hetaryl)ylidene derivatives of fluorinated 1,3-benzothiazin-4-ones

A series of 2-hetaryl- and 2-(hetaryl)ylidene substituted 5-fluoro-8-nitro-1,3-benzothiazin-4-ones was synthesized by interaction of 2,6-difluoro-3-nitrobenzoylisothiocyanate with C-nucleophiles. Cyclocondensation of polyfluorobenzoylchlorides with aryl and hetaryl thioamides represents new approach to 1,3-benzothiazin-4-ones. Some compounds proved to be promising for further development of tuberculostatic agents.

Keywords: 1,3-benzothiazin-4-ones; 2-fluorobenzoylchloride; 2-fluorobenzoyl-isothiocyanate; indole; pyrrole; cyanomethylbenzimidazole; benzoylmethylbenzimidazole; thioamide; cyclocondensation; tuberculostatics.

Received: 28.06.2020. Accepted: 25.08.2020. Published: 07.10.2020.

Introduction

Many synthetic benzothiazines are biologically actives, which play an important role in treatment of various diseases. Some 2-amino substituted 1,3-benzothiazin-4-ones (2-amino-1,3-benzothiazinones) represent a promising new class of antitubercular agents [1]. Other 1,3-benzothiazin-4-one derivatives, mostly 2-aryl and 2-(pyridin-2-yl) ones, are attractive due to their ability to suppress an oxidative stress-induced cardiomyocyte apoptosis [2]. Synthetic approaches to 2-amino-1,3-benzothiazin-4-ones are sufficiently developed, whereas not many ones are available for incorporation of C–C bond into position 2 [3]. The synthetic methods are limited to the following:

- interaction of 2-mercaptobenzoic acids with aryl/hetaryl nitriles [2];
- rearrangement of N-arylthiomethylaroylamides catalyzed by phosphorus oxychloride, followed by oxidation of 4*H*-1,3-benzothiazines with potassium permanganate [4];
- addition of C-nucleophiles to 2-fluorobenzoylisothiocyanates and subsequent intramolecular condensation [5].

The last approach opens wide opportunities for modification of position 2 of 1,3-benzothiazin-4-ones. Previously we

studied the interaction of polyfluorobenzoylisothiocyanates with CH-reactive benzimidazoles [5], 2,6-difluorobenzoylisothiocyanate with the same benzimidazoles and 2-cyanomethylpyridine [6], *o*-fluorobenzoylisothiocyanates with N-methylpyrrole and N-methylindole [7]. We presented only one example of 2-indolyl-5-fluoro-8-nitro-1,3-benzothiazin-4-one in recent paper [8].

In this article, we wish to report new data on 2-substituted 5-fluoro-8-nitro-1,3-benzothiazinones and introduce efficient synthetic approach to 2-aryl/hetaryl derivatives of 1,3-benzothiazin-4-ones based on cyclocondensation of polyfluorobenzoyl chlorides with thioamides.

Experimental

^{1}H and ^{19}F NMR (nuclear magnetic resonance) spectra were recorded in dimethylsulfoxide-d_6 (DMSO-d_6) on the spectrometer "Bruker-Avance-400" (400 MHz), using tetramethylsilane as internal reference for ^{1}H NMR and $CFCl_3$ for ^{19}F NMR. Mass spectra were recorded on a SHIMADZU GCMS-QP2010 Ultra instrument with electron impact ionization (EI) of the sample. Microanalyses (C, H, N) were performed using the Perkin — Elmer 2400 elemental analyzer. Melting points were measured on the Stuart melting point apparatus SMP10 (AC/DC input 230 V AC, Merck supplier).

2,6-Difluorobenzoic acid **1**, 2,3,4,5-tetrafluorobenzoyl chloride **10a** and pentafluorobenzoyl chloride **10b** were purchased from Merck (CAS numbers 385-00-2, 94695-48-4, 2251-50-5). 3-Nitro-2,6-difluorobenzoic acid **2** was synthesized according to the literature [9]. Procedure for toluene solution of 2,6-difluoro-3-nitrobenzoylchloride **3** was reported [8]. 2-Benzoylmethylbenzimidazole was prepared from 2-methylbenzimidazole [5], 2-cyanomethyl-benzimidazole was synthesized by condensation of ethyl cyanoacetate with *o*-phenylenediamine [10]. Thioamides **11** were prepared by the addition of hydrogen sulfide to the corresponding nitriles [11].

5-Fluoro-8-nitro-2-(1-methylpyrrol-2-yl) — 1,3-benzothiazin-4-one (5). The solution of ammonium isothiocyanate (0.4758 g, 6.26 mmol) in acetonitrile (10 mL) was added to toluene solution of 2,6-difluoro-3-nitrobenzoylchloride **3** (0.88 mL, 6.26 mmol). Reaction mixture was stirred at 40 °C for 5 min, the precipitate of NH_4Cl was filtered off and 1-methylpyrrole (0.761 g, 9.39 mmol) was added to a solution of 2,6-difluoro-3-nitrobenzoylisothiocyanate **3.** The mixture was stirred at room temperature for 3 h, the precipitate of benzothiazinone **5** was filtered off and washed with hot ethanol (10 mL). Yield 1.72 g (90%), mp 194–196 °C. ^{1}H NMR, δ (ppm), *J* (Hz): 4.09 s (3H, CH_3), 6.30 dd (1H, $H^{4'}$, $^{3}J_{HH}$ 4.1, $^{4}J_{HH}$ 2.3), 7.29 dd (1H, $H^{3'}$, $^{3}J_{HH}$ 4.2, $^{4}J_{HH}$ 1.3), 7.37 m (1H, $H^{5'}$), 7.62 dd (1H, H^{6}, $^{3}J_{HH}$ 9.2, $^{3}J_{FH}$ 9.4), 8.70 dd (1H, H^{7}, $^{3}J_{HH}$ 9.2, $^{4}J_{FH}$ 4.5). ^{19}F NMR, δ (ppm), *J* (Hz): — 99.05 dd (1F, $^{3}J_{FH}$ 9.5, $^{4}J_{FH}$ 4.0). MS (EI), *m/z* (I_{rel} (%)): 305 $[M]^+$ (14), 106 (100), 105 (15). Found, %: C 51.17; H 2.60; N 13.74. $C_{13}H_8FN_3O_3S$. Calculated, %: C 51.15; H 2.64; N 13.76.

Compounds **6–9** were synthesized by the same method.

5-Fluoro-8-nitro-2-(5-methoxy-1-methylindol-3-yl) — 1,3-benzothiazin-4-one (6). Yield 80%, mp 274–276 °C. ^{1}H NMR, δ (ppm), *J* (Hz): 3.83 s (3H, NCH_3), 3.93 s (3H, OCH_3), 7.01 d (1H, $H^{6'}$, $^{3}J_{HH}$

8.8), 7.54 d (1H, $H^{7'}$, $^3J_{HH}$ 8.8), 7.65 dd (1H, H^6, $^3J_{HH}$ 9.3, $^3J_{FH}$ 9.5), 7.97 s (1H, $H^{4'}$), 8.66 s (1H, $H^{2'}$), 8.70 dd (1H, H^7, $^3J_{HH}$ 9.3, $^4J_{FH}$ 4.3). $^{19}F\{^1H\}$ NMR, δ (ppm): — 99.27 s. MS (EI), *m/z* (I_{rel} (%)): 385 $[M]^+$ (31), 187 (12), 186 (100), 171 (41), 143 (28). Found, %: C 56.13; H 3.15; N 10.87. $C_{18}H_{12}FN_3O_4S$. Calculated, %: C 56.10; H 3.14; N 10.90.

5-Fluoro-8-nitro-2-(2-methylindol-3-yl) — 1,3-benzothiazin-4-one (7). Yield 91%, mp 207–209 °C. ^1H NMR, δ (ppm), *J* (Hz): 2.87 s (3H, CH_3), 7.25 m (2H, C_6H_4), 7.45 m (1H, C_6H_4), 7.66 dd (1H, H^6, $^3J_{HH}$ 9.3, $^3J_{FH}$ 9.6), 8.34 m (1H, C_6H_4), 8.71 dd (1H, H^7, $^3J_{HH}$ 9.3, $^4J_{FH}$ 4.6), 12.5 br. s (1H, NH). $^{19}F\{^1H\}$ NMR, δ (ppm): — 98.42 s. MS (EI), *m/z* (I_{rel} (%)): 355 $[M]^+$ (21), 157 (12), 156 (100), 155 (50), 81 (10). Found, %: C 57.43; H 2.82; N 11.85. $C_{17}H_{10}FN_3O_3S$. Calculated, %: C 57.46; H 2.84; N 11.83.

1-(1,3-Dihydrobenzimidazol-2-yliden) — 1-(5-fluoro-8-nitro-4-oxo-4*H*-1,3-benzothiazin-2-yl) — acetonitrile (8). Yield 75%, mp 319–321 °C. ^1H NMR, δ (ppm), *J* (Hz): 7.30 m (2H, C_6H_4), 7.50 dd (1H, H^6, $^3J_{HH}$ 9.2, $^3J_{FH}$ 9.8), 7.64 m (2H, C_6H_4), 8.62 dd (1H, H^7, $^3J_{HH}$ 9.2, $^4J_{FH}$ 4.4), 13.31 br. s (2H, NH). $^{19}F\{^1H\}$ NMR, δ (ppm): — 97.49 s. MS (EI), *m/z* (I_{rel} (%)): 381 $[M]^+$ (39), 183 (13), 182 (100), 155 (12), 103 (23), 81 (12). Found, %: C 53.50; H 2.15; N 18.36. $C_{17}H_8FN_5O_3S$. Calculated, %: C 53.54; H 2.11; N 18.37.

2-(1,3-Dihydrobenzimidazol-2-yliden) — 2-(5-fluoro-8-nitro-4-oxo-4*H*-1,3-benzothiazin-2-yl) — acetophenone (9). Yield 89%, mp 265–267 °C. ^1H NMR, δ (ppm), *J* (Hz): 7.36 m (5H, C_6H_5), 7.53 m (4H, C_6H_4), 7.60 dd (1H, H^6, $^3J_{HH}$ 9.2, $^3J_{FH}$ 9.5), 8.56 dd (1H, H^7, $^3J_{HH}$ 9.2, $^4J_{FH}$ 4.5), 13.36 br. s (2H, NH). $^{19}F\{^1H\}$ NMR, δ (ppm): — 98.39 s. MS (EI), *m/z* (I_{rel} (%)): 460 $[M]^+$ (24), 432 (13), 431 (41), 355 (25), 261 (46), 260 (100), 206 (16), 156 (16), 105 (45), 77 (71), 51 (10). Found, %: C 60.03; H 2.83; N 12.20. $C_{23}H_{13}FN_4O_4S$. Calculated, %: C 60.00; H 2.85; N 12.17.

6,7,8-Trifluoro-2-phenyl-1,3-benzothiazin-4-one (12a). Tetrafluorobenzoylchloride **10a** (0.85 g, 4 mmol) was added to thiobenzamide **11a** (0.397 g, 2.9 mmol) in dry toluene (8 mL), reaction mixture was refluxed for 3 h and then cooled. The precipitate of benzothiazinone **12a** was filtered off and recrystallized from DMSO. Yield 0.646 g (76%), mp 160–162 ^{0}C. ^1H NMR, δ (ppm), *J* (Hz): 7.62 m (2H, Ph), 7.73 m (1H, Ph), 8.15 ddd (1H, H^5, ^3J 10.3, ^4J 7.4, ^5J 2.2), 8.19 m (2H, Ph). ^{19}F NMR, δ (ppm), *J* (Hz): 151.84 ddd (1F, F^7, ^3J 22.5, ^3J 21.5, ^4J 7.4), 135.10 ddd (1F, F^8, ^3J 21.5, ^4J 6.2, ^5J 2.2), 132.50 ddd (1F, F^6, ^3J 22.5, ^3J 10.3, ^4J 6.2). MS (EI), *m/z* (I_{rel} (%)): 293 $[M]^+$ (11), 190 (100), 162 (30). Found, %: C 57.51, H 1.88, N 4.62. $C_{14}H_6F_3NOS$. Calculated, %: C 57.34, H 2.06, N 4.78.

Compounds **12b-h** were synthesized by the same method.

6,7,8-Trifluoro-2-(*p*-chlorophenyl) — 1,3-benzothiazin-4-one (12b). Yield 59%, mp 204–206 ^{0}C. ^1H NMR, δ (ppm), *J* (Hz): 7.73 d (2H, $H^{3',5'}$, ^3J 8.8), 8.23 d (2H, $H^{2',6'}$, ^3J 8.8), 8.24 ddd (1H, H^5, ^3J 10.6, ^4J 7.5, ^5J 2.1). ^{19}F NMR, δ (ppm), *J* (Hz): 151.68 ddd (1F, F^7, ^3J 22.5, ^3J 21.2, ^4J 7.5), 135.02 ddd (1F, F^8, ^3J 21.5, ^4J 6.3, ^5J 2.1), 132.29 ddd (1F, F^6, ^3J 22.5, ^3J 10.6, ^4J 6.3). MS (EI), *m/z* (I_{rel} (%)): 327 $[M]^+$ (4), 190 (100), 162 (27). Found, %: C 51.42, H 1.66, N 4.13. $C_{14}H_5F_3NOSCl$. Calculated, %: C 51.31, H 1.54, N 4.27.

6,7,8-Trifluoro-2-(*p*-tolyl) — 1,3-benzothiazin-4-one (12c). Yield 71%, mp 184–186 ^{0}C. ^1H NMR, δ (ppm), *J* (Hz): 2.46 s (3H, CH_3), 7.43 d (2H, $H^{3',5'}$, ^3J 8.0), 8.09 d (2H, $H^{2',6'}$, ^3J 8.0), 8.14 ddd (1H, H^5, ^3J 10.0, ^4J 7.5, ^5J 2.3). Found, %: C 58.75, H 2.70, N 4.41. $C_{15}H_8F_3NOS$. Calculated, %: C 58.63, H 2.62, N 4.56.

6,7,8-Trifluoro-2-(pyridyl-2) — 1,3-benzothiazin-4-one (12d). Yield 76%, mp 166–168 ^{0}C. ^{1}H NMR, δ (ppm), *J* (Hz): 7.75 dd (1H, $H^{5'}$, ^3J 8.0, ^3J 4.0), 8.10 td (1H, $H^{4'}$, ^3J 8.0, ^4J 1.8), 8.13 ddd (1H, H^5, ^3J 10.4, ^4J 7.4, ^5J 2.2), 8.38 d (1H, $H^{3'}$, ^3J 8.0), 8.79 dd (1H, $H^{6'}$, ^3J 4.0, ^4J 1.8). ^{19}F NMR, δ (ppm), *J* (Hz): 151.95 ddd (1F, F^7, ^3J 22.5, ^3J 21.1, ^4J 7.4), 135.64 ddd (1F, F^8, ^3J 21.1, ^4J 6.2, ^5J 2.2), 132.70 ddd (1F, F^6, ^3J 22.5, ^3J 10.4, ^4J 6.2). Found, %: C 52.95, H 1.63, N 9.67. $C_{13}H_5F_3N_2OS$. Calculated, %: C 53.06, H 1.71, N 9.52.

5,6,7,8-Tetrafluoro-2-phenyl-1,3-benzothiazin-4-one (12e). Yield 80%, mp 165–167 ^{0}C. ^{1}H NMR, δ (ppm), *J* (Hz): 7.63 m (2H, Ph), 7.76 m (1H, Ph), 8.17 m (2H, Ph). MS (EI), *m/z* (I_{rel} (%)): 311 $[M]^+$ (7), 208 (100), 180 (24), 111 (5). Found, %: C 53.83, H 1.81, N 4.67. $C_{14}H_5F_4NOS$. Calculated, %: C 54.02, H 1.62, N 4.50.

5,6,7,8-Tetrafluoro-2-(*p*-chlorophenyl) — 1,3-benzothiazin-4-one (12f). Yield 62%, mp 186–188 ^{0}C. ^{1}H NMR, δ (ppm), *J* (Hz): 7.66 d (2H, $H^{3',5'}$, ^3J 8.8), 8.20 d (2H, $H^{2',6'}$, ^3J 8.8). Found, %: C 48.83, N 3.97. $C_{14}H_4F_4NOSCl$. Calculated, %: C 48.64, H 1.17, N 4.05.

5,6,7,8-Tetrafluoro-2-(*p*-tolyl) — 1,3-benzothiazin-4-one (12g). Yield 74%, mp 191–193 ^{0}C. ^{1}H NMR, δ (ppm), *J* (Hz): 2.46 s (3H, CH_3), 7.43 d (2H, $H^{3',5'}$, ^3J 8.4), 8.08 d (2H, $H^{2',6'}$, ^3J 8.4). Found, %: C 55.46, H 2.24, N 4.19. $C_{15}H_7F_4NOS$. Calculated, %: C 55.39, H 2.17, N 4.31.

5,6,7,8-Tetrafluoro-2-(pyridyl-2) — 1,3-benzothiazin-4-one (12h). Yield 77%, mp 182–184 ^{0}C. ^{1}H NMR, δ (ppm), *J* (Hz): 7.76 ddd (1H, $H^{5'}$, ^3J 8.0, ^3J 4.8, ^4J 0.8), 8.10 td (1H, $H^{4'}$, ^3J 8.0, ^4J 1.8), 8.36 dd (1H, $H^{3'}$, ^3J 8.0, ^4J 0.8), 8.79 dd (1H, $H^{6'}$, ^3J 4.8, ^4J 1.8). Found, %: C 49.92, N 9.09. $C_{13}H_4F_4N_2OS$. Calculated, %: C 50.01, H 1.29, N 8.97.

Results and discussion

We developed an efficient synthetic approach to 2-hetaryl/(hetaryl)ylidene-substituted fluorinated 1,3-benzothiazinones, for this purpose we studied the interaction of the range of C-nucleophiles (indoles, N-methylpyrrole, 2-cyanomethyl- and 2-benzoylmethyl- benzimidazoles) with 2,6-difluoro-3-nitrobenzoylisothiocyanate **4** in acetonitrile at room temperature (Figure 1). According to ^{1}H and ^{19}F NMR spectra, the reaction leads to the formation of 1,3-benzothiazin-4-ones **5–9**, the intermediate addition products were not isolated, and fluorine atom at C^5 was not subjected to substitution with nucleophilic reagent. It is worth noting that the intramolecular cyclization proceeded at milder reaction conditions than in the case of 2,6-difluoro- and 2,3,4,5-tetrafluorobenzoyl derivatives (refluxing in acetonitrile or dimethylformamide in the presence of trimethylamine [7]).

The signals of H^6 and H^7 in ^{1}H NMR spectra of benzothiazinones **5–9** exhibit more complicated multiplicity than in the case of 2,5-diaminobenzothiazinones [8], which indicates that the fluorine atom remains in position 5. To prove that the alternative product of cyclization, 5-fluoro-6-nitro isomer, was not formed ^{19}F NMR spectra without suppression of F-H spin-spin interaction were registered. In such spectra of compounds **5–9** double doublet signals with $^3J_{FH}$ = 9.5–10.1 Hz and $^4J_{FH}$ = 3.9–4.0 Hz are present, so the formation of 5-fluoro-8-nitroisomers was confirmed. The peaks of molecular ions in the mass spectra of benzothiazinones **5–9** have a relative intensity of 14–39%.

Thus, we demonstrated the difference in behavior of C-nucleophiles and N-nucleophiles under the reaction with 2,6-difluoro-3-nitrobenzoylisothiocyanate **4**: application of C-nucleophiles allows to obtain derivatives of 5-fluoro-8-nitrobenzothiazinone, whereas the reaction with cycloalkylimines fails to avoid the nucleophilic substitution of fluorine at position 5. The proposed strategy opens wide opportunities for varying the substituent at position 2 of 8-nitrobenzothiazin-4-ones.

We presented novel one-stage synthetic approach to 2-substituted fluorine-containing 1,3-benzothiazin-4-ones based on cyclocondensation of polyfluorobenzoyl chlorides with thioamides as S,N-dinucleophiles. New 6,7,8-trifluoro- and 5,6,7,8-tetrafluoro-derivatives of 1,3-benzothiazin-4-ones **12a-h** were obtained by the reaction of polyfluorobenzoylchlorides **10a,b** and thioamides **11a-d** in boiling toluene for 3 h in 59–80% yields (Figure 2), notably that intermediate N-aroylation products were not isolated. Signals of NH groups are absent in ^{1}H NMR spectra of compounds **12a-h**, spectra of 6,7,8-trifluorobenzothiazinones **12a-d** exhibited ddd signal of fluoroarene residue H^{5} proton at 8.13–8.24 ppm. The number of signals in ^{19}F NMR spectra is in accordance with the structure of benzothiazinones **12**. The peaks of molecular ions in the mass

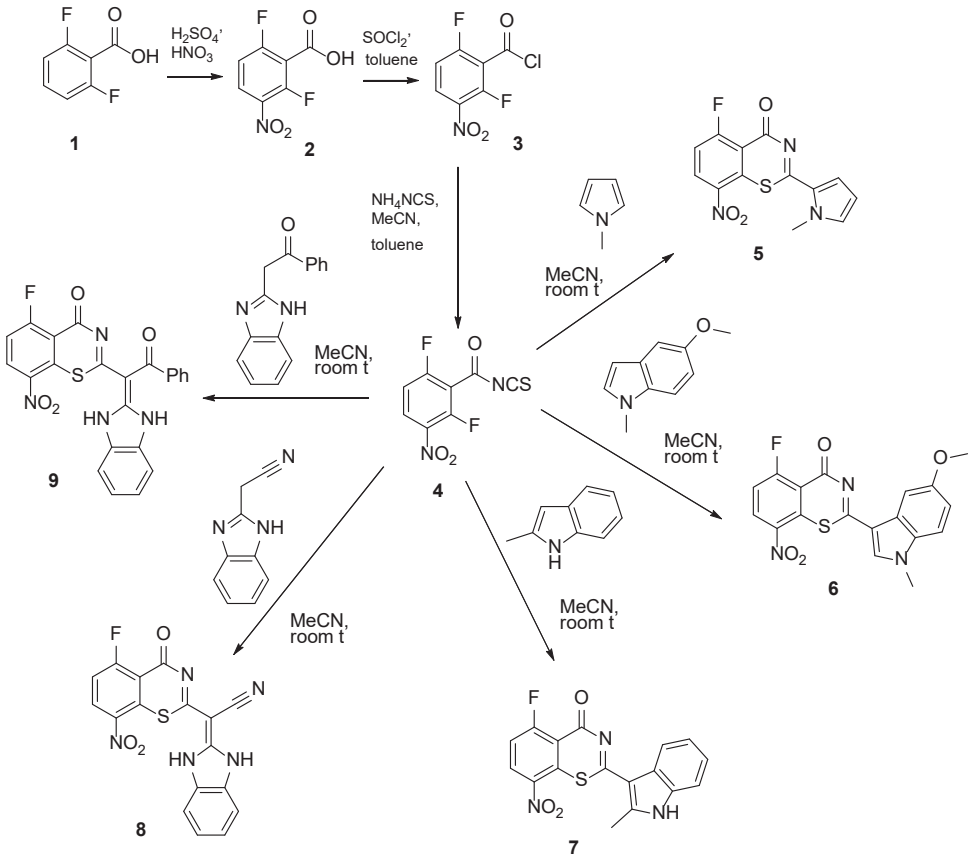

Fig. 1. Synthesis of 5-fluoro-8-nitro-1,3-benzothiazin-4-ones **5–9**

spectra of benzothiazinones **12** have low relative intensity of 4–11%. The ions *m*/*z* 190 or *m*/*z* 208 with 100% intensity were observed for benzothiazinones **12,** moreover, peaks *m*/*z* 162 or *m*/*z* 180 correspond to ions $[M\text{-}RCN\text{-}CO]^+$. The most abundant peak was reported to be characteristic for elimination of RCN fragment from molecular ions of 2-R-6,7,8-trifluoro-1,3-benzothiazin-4-ones [5–7].

The presented approach allows to obtain a variety of 2-aryl/hetaryl-substituted 1,3-benzothiazinones and successfully complements the previously described cyclocondensation of polyfluorobenzoylchlorides with benzimidazol-2-thiones as cyclic S,N-dinucleophiles leading to [*b*]-annelated fluorobenzothiazinones [12]. Unfortunately, we failed to obtain 5-fluoro- and 5-fluoro-8-nitro analogs using the method shown in Figure 2.

Tuberculostatic activity of polyfluorinated benzothiazinnes **12** was studied at two laboratories, namely Ural Research Institute for Phthisiopulmonology (URIP) and University of Illinois, Chicago Institute for Tuberculosis Research (INR); the data are presented in Table 1.

Table 1

Data on tuberculostatic activity of fluorinated 2-aryl/pyridyl-1,3-benzothiazin-4-ones 12 against *Mycobacterium tuberculosis* $H_{37}R_v$*

Comp	MIC values (URIP data), μg/mL	% Inhibition at 128 μg/mL (ITR data)		MIC values, μg/mL (ITR data)		IC_{50}, μg/mL (ITR data)
		MABA	LORA	MABA	LORA	
12b	12.5	28	66	-	-	—
12c	12.5	95	100	58.0	52.3	>128
12d	0.3	—	—	>128	>128	—
12f	3.12	0	100	—	**3.7**	53.5
12g	nd	74	99	—	26.3	—
12h	12.5	0	100	—	55.8	65.9

* MIC–Minimal inhibitory concentration; IC_{50} — the half maximal inhibitory concentration; URIP — Ural Research Institute for Phthisiopulmonology; INR — Chicago Institute for Tuberculosis Research; MABA — microplate Alamar Blue assay; LORA — low-oxygen recovery assay.

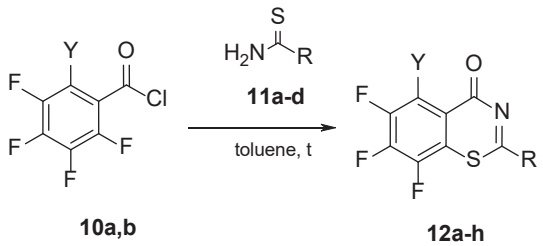

10: Y = H (**a**), F (**b**); **11**: R = Ph (**a**), 4-Cl-C_6H_4 (**b**), 4-Me-C_6H_4 (**c**), 2-Py (**d**); **12**: Y = H, R = Ph (**a**), 4-Cl-C_6H_4 (**b**), 4-Me-C_6H_4 (**c**), 2-Py (**d**); Y = F, R = Ph (**e**), 4-Cl-C_6H_4 (**f**), 4-Me-C_6H_4 (**g**), 2-Py (**h**).

Fig. 2. Synthesis of polyfluorinated 2-aryl/pyridyl-1,3-benzothiazin-4-ones **12a-h**

According to trials conducted in URIP, benzothiazinone **12d** exhibited the highest activity (MIC 0.3 μg/mL, isoniazide as reference compound with MIC 0.15 μg/mL). Data obtained in ITR revealed **12f** as the most promising derivative towards the dormant multi-resistant strain of micobacteria $H_{37}R_V$–CA-luxAB (MIC 3.7 μg/mL, rifampicinum as reference compound with MIC 8.26 μg/mL).

Conclusions

To sum up, we developed efficient synthetic approaches to fluorine-containing 1,3-benzothiazin-4-ones bearing aryl, hetaryl and (hetaryl)ylidene residues at position 2 and demonstrate that some of them are promising for design of new antitubercular agents.

Acknowledgements

The work was carried out with financial support from the Ministry of Science and Higher Education of Russian Federation (project № FEUZ-2020–0058 (H687.42Б.223/20)).

References

1. Chetty S, Ramesh M, Singh-Pillay A, Soliman M. Recent advancements in the development of anti-tuberculosis drugs. Bioorg Med Chem Lett. 2017;27(3):370–86. DOI: 10.1016/j.bmcl.2016.11.084
2. Kimura H, Sato Y, Tajima Y, Suzuki H, Yukitake H, Imaeda T, Kajino M, Oki H, Takizawa M, Tanida S. BTZO-1, a Cardioprotective Agent, Reveals that Macrophage Migration Inhibitory Factor Regulates ARE-Mediated Gene Expression. Chem Biology. 2010;17(12):1282–94. DOI: 10.1016/j.chembiol.2010.10.011
3. Nosova EV, Lipunova GN, Charushin VN, Chupakhin ON. Synthesis and biological activity of 2-amino- and 2-aryl(hetaryl) substituted 1,3-benzothiazin-4-ones. Mini-Reviews in Medicinal Chemistry. 2019;19(12):999–1014. DOI: 10.2174/1389557518666181015151801
4. Szabo J, Bani-Akoto E, Dombi G, Gunther G, Bernath G, Fodor L. Ring-closure reaction of N-arylthiomethylaroylamides to 1,3-benzothiazines. J. Heterocyc. Chem. 1992;29(5):1321–4. DOI:10.1002/jhet.5570290545
5. Nosova EV, Lipunova GN, Laeva AA, Charushin VN. Polyfluorobenzoyl chlorides and isothiocyanates in reactions with CH-reactive benzimidazoles. Russ. Chem. Bull. 2005;54(3):733–7. DOI: 10.1007/s11172-005-0312-6
6. Nosova EV, Laeva AA, Trashakhova TV, Golovchenko AV, Lipunova GN, Slepukhin PA, Charushin VN. Fluorine-containing heterocycles: XVIII. Monofluoro derivatives of quinazolines and 1,3-benzothiazin-4-ones. Russ J Org Chem. 2009;45(6):904–12. doi:10.1134/S1070428009060189

7. Nosova EV, Poteeva AD, Lipunova GN, Slepukhin PA, Charushin VN. Synthesis of Fluorine-Containing 2-Pyrrolyl- and 2-Indolyl-Substituted 1,3-Benzothiazin-4-ones. Russ J Org Chem. 2019;55(3):384–7.
DOI: 10.1134/S1070428019030205
8. Nosova EV, Batanova OA, Lipunova GN, Charushin VN. Synthesis of novel 8-nitro-substituted 1,3-benzothiazin-4-ones. Mendeleev Communications. 2020;30(4);427–9.
DOI: 10.1016/j.mencom.2020.07.007
9. Yoshida Y, Barrett D, Azami H, Morinaga C, Matsumoto S, Matsumoto Y, Takasugi H. Studies on Anti-Helicobacter pylori Agents. Part 1: Benzyloxyisoquinoline Derivatives. Bioorg Med Chem. 1999;7(11):2647–66.
DOI: 10.1016/S0968-0896(99)00203–5
10. Mohareb RM, Abdallah AEM, Mohamed AA. Synthesis of Novel Thiophene, Thiazole and Coumarin Derivatives Based on Benzimidazole Nucleus and Their Cytotoxicity and Toxicity Evaluations. Chem Pharm Bull. 2018;66(3):309–18.
DOI: 10.1248/cpb.c17–00922
11. Mochul'skaya NN, Andreiko AA, Kodess MI, Vasil'eva EB, Filyakova V. I, Gubaidullin AT, Litvinov IA, Sinyashin OG, Aleksandrov GG, Charushin VN. Annelation of the thiazole ring to 1,2,4-triazines by tandem A_N-A_N or S_N^H-S_N^H reactions. Russ Chem Bull, Int Ed. 2004;53(6):1279–89.
DOI: 10.1023/B:RUCB.0000042287.32992.54
12. Lipunova GN, Nosova EV, Mokrushina GA, Ogloblina EG, Aleksandrov GG, Charushin VN. Fluorocontaining Heterocycles: IX. Derivatives of Imidazo[2,1-*b*][1,3]benzothiazine. Russ J Org Chem. 2003;39(2):248–56.
DOI: 10.1023/A:1025548505109

DOI: 10.15826/chimtech.2020.7.3.02

M. I. Savchuk [a], E. S. Starnovskaya [ab], Y. K. Shtaitz [a], A. P. Krinochkin [ab], D. S. Kopchuk [ab], S. Santra[a], M. Rahman[a], G. V. Zyryanov [ab], V. L. Rusinov [ab], O. N. Chupakhin[ab]

[a] *Ural Federal University named after the first President of Russia B. N. Yeltsin, 620002, 19 Mira St., Ekaterinburg, Russia*

[b] *I. Ya. Postovsky Institute of Organic Synthesis of RAS (Ural Branch), 620990, 22/20 S. Kovalevskoy/Akademicheskaya St., Ekaterinburg, Russia*

**email: g.v.zyrianov@urfu.ru*

Direct synthesis of 5-arylethynyl-1,2,4-triazines via direct CH-functionalization

An efficient synthetic approach towards 5-arylethynyl-1,2,4-triazines via direct C-H-functionalization of 5-*H*-1,2,4-triazines in reaction with lithium acetylenes is reported.

Keywords: C-H-Functionalization, 1,2,4-triazines; acetylenes lithium salts; 5-arylethynyl-1,2,4-triazines

Received: 05.08.2020. Accepted: 01.09.2020. Published: 07.10.2020.

Introduction

Heterocyclic acetylenes are widely used in various heterocyclization reactions [1], especially via click reactions [2]. Acetylene spacers are presented in a number of conjugated heterocyclic chromophores [3]. Additionally, some heterocyclic acetylenes are known posses with biological activities, for instance as antihypertensive agents [4].

The object of study of this work — 5-arylethynyl-1,2,4-triazines — are promising substrates for the preparation of various classes of compounds with unique applied properties. For example, by the transformation of the 1,2,4-triazine ring into the pyridine one via the aza-Diels-Alder reaction with vatious dienophiles, the corresponding pyridines can be obtained, including 2,2' — bipyridine ligands [4]. In addition, arylethynyl substituted 1,2,3-triazoles were obtained in the reaction of the corresponding 3- (2-pyridyl) — 1,2,4-triazines with aryne intermediates [5–6]. Also, by the chemical transformation of 5-arylethynyl the corresponding 5-phenacyl-1,2,4-triazines could be obtained [7–8], which in turn can be transformed into 5-methyl-1,2,4-triazines [9].

Among the reported methods for the synthesis of 5-arylethynyl-1,2,4-triazines, the use of the Sonogashira cross-coupling can be highlighted [10], and in this case 5-iodine or 5-chloro-1,2,4-triazines were used as reactants In addition, the direct introduction of an arylethynyl moiety via the C-H functionalization of 1,2,4-triazine-4-oxides in the reaction with the lithium salt of acetylene are described by using

deoxygenative aromatization pathway, and the benzoyl chloride was used as an acylating agent [5,11]. The interaction of non-activated 1,2,4-triazines with the lithium salt of arylacetylene is also described, however, the corresponding 5-styryl-1,2,4-triazines were the main reaction products [12–13]. In this aspect, it should be noted the greater availability of 1,2,4-triazines compare to 1,2,4-triazine-4-oxides; and the preparation of ethynyl derivatives starting from 1,2,4-triazines looks more attractive.

In this article, we wish to report an efficient synthesis of 5-arylethynyl-1,2,4-triazines **1** via direct C-H-functionalization of 5-*H*-1,2,4-triazines **2** with lithium arylacetylenes.

Experimental part

^{1}H NMR spectra were recorded on a Bruker Avance-400 spectrometer (400 MHz), the internal standard was $SiMe_4$. Mass spectra (ionization type — electrospray) were recorded on a MicrOTOF-Q II instrument from Bruker Daltonics (Bremen, Germany). Elemental analysis was performed on a Perkin Elmer PE 2400 II CHN analyzer. The starting 1,2,4-triazine **2** was obtained according to the described method [14].

A general procedure for the synthesis of of arylethynyl-1,2,4-triazines 1:

A solution of n-BuLi in hexane (2.5 M, 0.8 ml) was added to a solution of the corresponding arylacetylene (2 mmol) in dry THF (4 ml) in a Schlenk flask at a temperature of –78 °C in an argon atmosphere, and the resulting mixture was stirred for 5 min. Then the solution of the corresponding 1,2,4-triazine **1** (1.6 mmol) in dry toluene (35 ml) was added, and a minute later a solution of DDQ (305 mg, 1.34 mmol) in dry toluene (10 ml) was added. The resulting mixture was stirred for 3 h at 78 °C to room temperature. After that methanol (10 ml) was added, and the reaction mixture stirred for 5 min and the solvents were removed under reduced pressure. The resulting oily residue was purified by column chromatography (neutral alumina, eluent: dichloromethane) to afford the desired products.

3- (2-Pyridyl) — 6-phenyl-5-phenylethynyl-1,2,4-triazine (1a). Yield 565 mg (1.7 mmol, 85%). Rf 0.6. M.p. 142–144 °C. NMR ^{1}H ($CDCl^3$, δ, ppm): 7.37–7.41 (m, 2H, PhC≡C), 7.43–7.55 (m, 4H, PhC≡C, H-5 (py)), 7.59–7.63 (m, 3H, Ph), 7.94–7.99 (ddd, 1H, ^3J 8.0, 8.0 Hz, ^4J 2.0 Hz, H-4 (py)), 8.19–8.22 (m, 2H, Ph), 8.75 (dd, 1H, ^3J 8.0 Hz, ^4J 1.0 Hz, H-3 (py)), 8.96 (dd, 1H, ^3J 4.8 Hz, ^4J 2.0 Hz, H-6 (py)). ^{13}C NMR ($CDCl_3$, δ, ppm): 86.5 (C-sp), 100.8 (C-sp), 120.8, 124.2, 125.7, 128.5, 128.7, 129.5, 130.7, 132.6, 133.9, 137.2, 142.6, 150.6, 152.4, 157.7, 160.7. ESI–MS, m/z: 335.13 $(M + H)^+$. Found, %: C 78.82, H 4.01, N 16.55. $C_{22}H_{14}N_4$. Calculated, %: C 79.02, H 4.22, N 16.76.

5 - ((4-Methoxyphenyl) ethynyl) — 3- (pyridin-2-yl) — 6-phenyl-1,2,4-triazine (1b). Yield 515 mg (1.41 mmol, 88%). NMR ^{1}H ($CDCl_3$, δ, ppm): 3.85 (m, 3H, OCH_3), 6.89 (m, 2H, C_6H_4), 7.45–7.54 (m, 3H, C_6H_4, H-5 (py)), 7.55–7.64 (m, 3H, Ph), 7.95 (ddd, 1H, ^3J 7.6 Hz, 7.6 Hz, ^4J 1.6 Hz, H-4 (py)), 8.17–8.23 (m, 2H, Ph), 8.74 (d, 1H, ^3J 8.0 Hz, H-3 (py)), 8.94 (d, 1H, ^3J 4.8 Hz, H-6 (py)). ESI–MS, m/z: 365.14 $(M + H)^+$. Found, %: C 75.70, H 4.30, N 15.25. $C_{23}H_{16}N_4O$. Calculated,%: C 75.81, H 4.43, N 15.37.

Results and discussion

The previously proposed mechanism [14] for the reaction of 1,2,4-triazines and lithium-acetylenes is presented on the scheme 1.

According to the mechanism, at the first stage, the corresponding σ^H-adduct **A** is formed, which further undergoes a 1,2-hydride shift affording the formation of the corresponding styryl substituent. And the treatment of the reaction mixture with methanol at the final stage leads to the products **3**. Obviously, to block the pathway A for the reaction, the σH-adduct A need to be treated with and oxidant to form 5-ethynyl-1,2,4-triazine **1**, which no longer turn into 5-styryl derivative 3 Indeed, it was found that the addition of an oxidizing agent, such as 2,3-dichloro-5,6-dicyanobenzoquinone (DDQ), 10 minutes after the initiation of the reaction between 1,2,4-triazine and the arylacetylene lithium salt allowed us to obtain the corresponding 5-phenylethynyl- 1,2,4-triazines 1 in up to 88% yields (way **B**), and they were isolated using column chromatography.

The structure of products **1** was confirmed based on the data of NMR ^{1}H, ^{13}C spectroscopy, mass spectrometry, and elemental analysis. Thus, in the ^{13}C NMR spectra, the signals of *sp*-hybrid carbon atoms in the range of 86.5–100.8 ppm can be observed. The spectral data of compound **1a** correspond to those previously published during its synthesis by an alternative method [5].

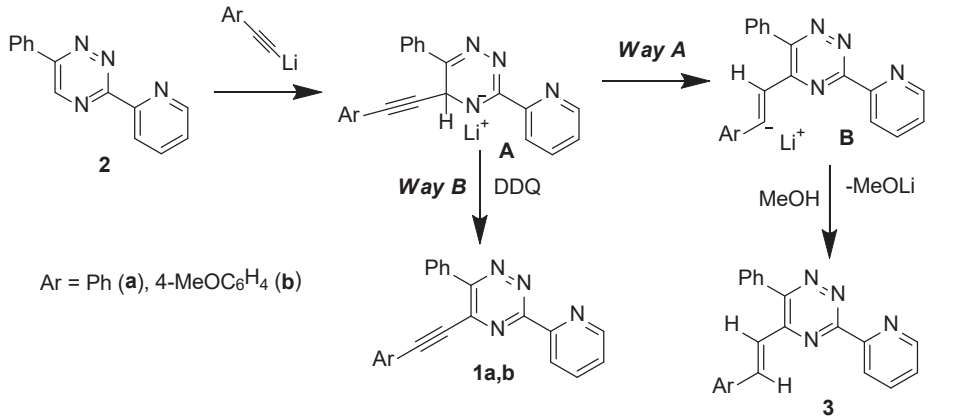

Scheme 1. Mechanism of reaction of 5-H-1,2,4-triazines 2 with lithium-acetylenes

Conclusions

An efficient synthetic approach towards 5-arylethynyl-1,2,4-triazines via direct C-H-functionalization of 5-H-1,2,4-triazines in reaction with lithium-acetylenes was reported. This method could serve as a possible *Pd-free* alternative to the Sonogashira cross-coupling.

Acknowledgements

This work was supported by the Russian Science Foundation (Grant # 20-13-00142) and Grants Council of the President of the Russian Federation (no. NSh-2700.2020.3).

References

1. a) Heravi MM, Sadjadi S. Recent advances in the application of the Sonogashira method in the synthesis of heterocyclic compounds. Tetrahedron. 2009;65:7761–7775. DOI: 10.1016/j.tet.2009.06.028 ; b) Verma AK, Jha RR, Chaudhary R, Tiwari RK, Reddy KSK, Danodia A. Copper-catalyzed tandem synthesis of indolo-, pyrrolo[2,1-a]isoquinolines, naphthyridines and bisindolo/pyrrolo[2,1-a]isoquinolines *via* hydroamination of ortho-haloarylalkynes followed by C-2 arylation. J Org Chem. 2012;77:8191–8205.
   DOI: 10.1021/jo301572p
2. a) Pasini D. The Click Reaction as an Efficient Tool for the Construction of Macrocyclic Structures. Molecules. 2013;18:9512–9530. DOI: 10.3390/molecules18089512 ; b) Hiroki H, Ogata K, Fukuzawa S-I. 2-Ethynylpyridine-promoted rapid copper(i) chloride catalyzed azide — alkyne cycloaddition reaction in water. Synlett. 2013;24:843–846.
   DOI: 10.1055/s-0032–1318488 ; c) Kovács S, Zih-Peréni K, Révész Á, Novák Z. Copper on iron: catalyst and scavenger for azide — alkyne cycloaddition. Synthesis. 2012;44:3722–3730.
   DOI: 10.1055/s-0032–1317697
3. a) Benniston AC, Harriman A, Lawrie DJ, Mayeux A, Rafferty K, Russell OD. A general purpose reporter for cations: absorption, fluorescence and electrochemical sensing of zinc(ii). Dalton Trans. 2003;4762–4769. DOI: 10.1039/B313413J ; b) Joshi HS, Jamshidi R, Tor Y. Conjugated 1,10-Phenanthrolines as Tunable Fluorophores. Angew Chem Int Ed. 1999;38:2722–2725.
   DOI: 10.1002/(SICI)1521–3773(19990917)38:18<2721::AID-ANIE2721>3.0.CO;2–5
4. John R. Carson, inventor; McNeilab, Inc., assignee. Heteroaromatic acetylenes useful as anthypertensive agents. US Patent 4,663,334. 1987.
5. Kozhevnikov DN, Kozhevnikov VN, Prokhorov AM, Ustinova MM, Rusinov VL, Chupakhin ON, Aleksandrov GG, König B. Consecutive nucleophilic substitution and aza Diels — Alder reaction — an efficient strategy to functionalized 2,2'-bipyridines. Tetrahedron Lett. 2006;47(6): 869–872.
   DOI: 10.1016/j.tetlet.2005.12.006
6. Kopchuk DS, Nikonov IL, Khasanov AF, Giri K, Santra S, Kovalev IS, Nosova EV, Gundala S, Venkatapuram P, Zyryanov GV, Majee A, Chupakhin ON. Studies on the interactions of 5-R-3-(2-pyridyl) — 1,2,4-triazines with arynes: inverse demand aza-Diels — Alder reaction versus aryne-mediated domino process. Org Biomol Chem. 2018;16:5119–5135.
   DOI: 10.1039/C8OB00847G
7. Kopchuk DS, Krinochkin AP, Khasanov AF, Kovalev IS, Slepukhin PA, Starnovskaya ES, Mukherjee A, Rahman M, Zyryanov GV, Majee A, Rusinov VL, Chupakhin ON, Santra S. An Efficient Cyanide-Free Approach towards 1-(2-Pyridyl) isoquinoline-3-carbonitriles *via* the Reaction of 5-Phenacyl-1,2,4-triazines with 1,2-Dehydrobenzene in the Presence of Alkyl Nitrites. Synlett. 2018;29:483–488.
   DOI: 10.1055/s-0036–1590961
8. Prokhorov AM, Slepukhin PA, Kozhevnikov DN. $CuCl_2$ induced reactions of 6-ethynyl- and 6-cyano-5-aryl-2,2' — bipyridines with various N- and O-nucleophiles

in comparison with the reactions of relative 1,2,4-triazines. J Organometallic Chem. 2008;693:1886–1894.
DOI: 10.1016/j.jorganchem.2008.02.016

9. Kopchuk DS, Nikonov IL, Krinochkin AP, Kovalev IS, Zyryanov GV, Rusinov VL, Chupakhin ON. One-pot non-cyanide synthesis of 1-(pyridin-2-yl)isoquinoline-3-carbonitrile by reaction of 1-phenyl-2-[6-phenyl-3-(pyridin-2-yl) — 1,2,4-triazin-5-yl]ethanone with 1,2-dehydrobenzene in the presence of isoamyl nitrite. Russ J Org Chem. 2017;53(6):959–961.
DOI: 10.1134/S1070428017060264
10. a) Krinochkin AP, Kopchuk DS, Kovalev IS, Zyryanov GV, Rusinov VL, Chupakhin ON. One-Step synthesis of 5-methyl-1,2,4-triazines by the transformation of their 5-phenacyl derivatives. Russ J Org Chem. 2019;55(2):266–268. DOI: 10.1134/S1070428019020210; b) Krinochkin AP, Kopchuk DS, Kim GA, Shevyrin VA, Santra S, Rahman M, Taniya OS, Zyryanov GV, Rusinov VL, Chupakhin ON. Water-soluble luminescent lanthanide complexes based on C6-DTTA-appended 5-aryl-2,2′-bipyridines. Polyhedron. 2020;181:114473.
DOI: 10.1016/j.poly.2020.114473
11. Shoetsu K, Satoshi F, Hiroshi Y. Studies on as-Triazine Derivatives. V. Synthesis and Hydration of Alkynyl-1,2,4-triazines. Heterocycles. 1984;22(10):2245–2248.
12. Prokhorov AM, Makosza M, Chupakhin ON. Direct introduction of acetylene moieties into azines by SNH methodology. Tetrahedron Lett. 2009;50(13):1444–1446.
DOI: 10.1016/j.tetlet.2009.01.070
13. Carroll FI, Kotturi SV, Navarro HA, Mascarella SW, Gilmour BP, Smith FL, Gabra BH, Dewey WL. Synthesis and pharmacological evaluation of phenylethynyl[1,2,4] methyltriazines as analogues of 3-methyl-6-(phenylethynyl)pyridine. J Med Chem. 2007;50(14):3388–3391.
DOI: 10.1021/jm070078r
14. Khasanov AF, Kopchuk DS, Kovalev IS, Taniya OS, Zyryanov GV, Rusinov VL, Chupakhin ON. Reaction of lithium 2-arylethynides with 6-aryl-3-(2-pyridyl) — 1,2,4-triazines as an access to 6-aryl-5-arylvinyl-3-(2-pyridyl) — 1,2,4-triazines. Mendeleev Commun. 2015;25(5):332–333.
DOI: 10.1016/j.mencom.2015.09.003
15. Kozhevnikov VN, Shabunina OV, Kopchuk DS, Ustinova MM, König B, Kozhevnikov DN. Facile synthesis of 6-aryl-3-pyridyl-1,2,4-triazines as a key step towards highly fluorescent 5-substituted bipyridines and their Zn(II) and Ru(II) complexes. Tetrahedron. 2008;64:8963–8973.
DOI: 10.1016/j.tet.2008.06.040

DOI: 10.15826/chimtech.2020.7.3.03

Yu. A. Azev,* O. S. Koptyaeva, O. S. Eltsov, Yu. A. Yakovleva, T. A. Pospelova

Ural Federal University
620002, 19 Mira St., Ekaterinburg, Russian Federation
**email: azural@yandex.ru*

New pathways for the synthesis of indolyl-containing quinazoline trifluoroacetohydrazides

The reactions of indole-3-carbaldehyde arylhydrazones with quinazoline in TFA proceed at the 7′ position of the aryl part of the hydrazone molecule to form σ-adducts of quinazoline trifluoroacetohydrazides.

Keywords: arylhydrazones; indole-3-carboxaldehydes; C,C-coupling; trifluoroacetyl quinazoline hydrazides.

Received: 19.08.2020. Accepted: 28.09.2020. Published: 07.10.2020.

Introduction

It is known that the quinazoline core is part of natural alkaloids [1, 2]. Among the quinazoline derivatives, compounds have been identified that have various types of biological activity, including antimicrobial, antiallergic, hypotonic, and antiviral [3]. Quinazoline derivatives have been synthesized, which have shown antitumor [4] and radioprotective activity [5].

The addition of C-nucleophiles to 3-methylquinazolinium iodide with the formation of 4-substituted 3,4-dihydroquinazolines has been reported [6]. It is also known that unsubstituted quinazoline reacts with indole, 3-methyl-1-phenylpyrazolone-5, 1,3-dimethylbarbituric acid, and pyrogallol in the presence of acid to form 4-σ-adducts [7]. Examples of arylation of quinazoline with 1,3,5-trimethoxybenzene, 1-(4-methoxybenzylidene) — 2-phenylhydrazine, and o-phenylenediamine derivatives have been described [8].

To create effective drugs based on quinazoline, it is important to be able to change substituents (pharmacophoric fragments) in the structure of the compound. Theoretically, this will allow to affect their physicochemical properties (hydrophilicity, lipophilicity, etc.), changing their bioavailability and activity.

Indole is part of tryptophan and its metabolites and this one is also present in a number of natural alkaloids and antibiotics [9]. Indole derivatives exhibit antitumor, antiviral, anti-inflammatory, antidepressant, and other types of activity [10].

This work is a continuation of research related to the development of methods for the synthesis of biologically active derivatives of quinazoline [7]. It should be noted that within the framework of this direction, atomic-economical reactions corresponding to the principles of green chemistry are a particular value [11]. This type of interactions includes nucleophilic reactions of C,C-coupling under conditions of acid catalysis, which proceed without using of metal catalysts and are theoretically waste-free [12,13].

Experimental section

Unless otherwise indicated, all common reagents and solvents were used from commercial suppliers without further purification.

The reaction progress and purity of the obtained compounds were controlled by TLC method on Sorbfil UV-254 plates, using visualization under UV light. Melting points were determined on a Stuart SMP10 melting point apparatus.

1H, 13C and 19F NMR spectra were acquired on Bruker Avance-400 and Bruker Avance NEO — 600 spectrometers in DMSO-d6 solutions, using TMS as internal reference for 1H and 13C NMR or $CFCl^3$ for 19F NMR. Mass-spectra (EI, 70eV) were recorded on MicrOTOF-Q instrument (Bruker Daltonics) at 250˚C.

*The general method for the reaction of indole carbaldehyde **1** with hydrazines **2a-2d***

2-Methyl-1*H*-indole-3-carbaldehyde **1** (0.5 mmol) was dissolved in ethanol (3 ml). Then this solution was added to mixture of the corresponding hydrazine **2** and hydrochloric acid (0.02 ml) in water (3.0 ml). The resulting mixture was refluxed for 5–10 minutes and then was cooled. The resulting solid was filter off and dried. The crude hydrazones were used directly in the next step without additional purification.

Spectral data for hydrazones **3a-c** were described earlier [14].

2-Methyl-3-{[2-(4-methylphenyl) hydrazono]methyl}-1*H*-indole (3d)

Yield 55%, mp 185–186°C. ^{1}H NMR spectrum (600 MHz, DMSO-d_6), δ, ppm: 2.21 s (3H, CH_3), 2.48 s (3H, C^2CH_3), 6.93 d (2H, *J* 8.4 Hz, H_o), 7.02 d (2H, *J* 8.4 Hz, H_m), 7.07–7.11 m (2H, H^5 and H^6), 7.30 m (1H, H^7), 8.12–8.15 m (2H, $H^{1'}$ and H^4), 9.61 br.s (1H, $N^{3'}H$), 11.19 s (1H, N^1H). MS, m/z (I_{rel},%): 263 (M^+, 100).

2-Methyl-3-[(2-phenylhydrazinyl) methyl]-1*H*-indole (3e). Yield 59%, m. p. 192–193 °C. ^{1}H NMR spectrum (600 MHz, DMSO-d_6), δ, ppm: 2.49 s (3H, CH_3), 6.67 t.t (1H, *J* 7.3, 1.2 Hz, H_p), 7.03 d.d (2H, *J* 8.5, 1.2 Hz, H_o), 7.08–7.12 m (2H, H^5, H^6), 7.21 d.d (2H, *J* 8.5, 7.3 Hz, H_m), 7.31 m (1H, H^7), 8.15 m (1H, H^4), 8.17 c (1H, $H^{1'}$), 9.78 br.s (1H, $N^{3'}H$), 11.23 s (1H, N^1H). ^{13}C NMR spectrum (151 MHz, DMSO-d_6), δ, ppm: 136.06 (C^2), 118.04 (C^3), 129.91 (C^{3a}), 130.99 (C^4), 127.76 (C^5), 127.49 (C^6), 127.78 (C^7), 132.84 (C^{7a}), 139.22 ($C^{1'}$), 139.44 (C_i), 124.4 (C_o), 129.27 (C_m), 127.67 (C_p), 115.98 (CF_3), 155.28 (C=O). ^{15}N NMR spectrum (61 MHz, DMSO-d_6), δ, ppm: 126.8 (N^1), 305 ($N^{3'}$), 218.5 ($N^{3'}$). MS, m/z (I_{rel},%): 249 (M^+, 100).

*The general method for the reaction of hydrazones **3d-3e** with quinazoline **4***

A mixture of quinazoline **4** (0.5 mmol) and the corresponding hydrazone **3d,e** in TFA (3.0 ml) was refluxed for 65–70 h. The solvent was removed under reduced pressure. Water (2.0 ml) was added to the residue; the solid was filtered off. The resulting product **6a,b** was analytically pure and no additional purification was required.

4-(4-(2-((1*H*-indol-3-yl)methylene) — 1-(2,2,2-trifluoroacetyl)hydrazinyl)phenyl) — 1,4-dihydroquinazolinium-3 2,2,2- trifluoroacetate (6a). Yield 51%, m.p. 112–113 °C. ^{1}H NMR spectrum (600 MHz, DMSO-d_6), δ, ppm: 6.24 s (1H, $H^{4''}$), 7.07 d (1H, *J* 7.4 Hz, $H^{5''}$), 7.20–7.24 m (2H, $H^{6''}$, $H^{7''}$), 7.37 t (1H, *J* 7.7 Hz, 1H, H^5), 7.41 d (1H, *J* 6.7 Hz, H^4), 7.43–7.45 m (2H, $H^{6,7}$), 7.61 d

(2H, *J* 8.4 Hz, $H^{5'}$), 7.69 d (2H, *J* 7.6 Hz, $H^{8''}$), 7.92 d (2H, *J* 8.4 Гц, $H^{6'}$), 7.98 s (1H, $H^{1'}$), 8.57 s (1H, $H^{2''}$), 8.80 s (1H, H^2), 11.18 s (2H, N^1H, $N^{3''}H$), 12.37 s (1H, COOH). 13C NMR spectrum (151 MHz, DMSO-d_6), δ, ppm: 54.61 ($C^{4''}$), 116.39 q (1C, *J* 288.7 Hz, CF_3), 117.59 ($C^{8''}$), 119.17 (C^3), 121,42 ($C^{6'}$), 122.42 (C^{4a}), 126.86 (C^7), 127.83 ($C^{6''}$), 128.22 ($C^{7'}$), 128.60 ($C^{5'}$), 128.73 ($C^{5''}$), 129.34 ($C^{7''}$), 129.48 (C^4), 129.82 (C^{8a}), 130.07 (C^{3a}), 131.90 (C^{7a}), 132.0 ($C^{4'}$), 139.89 (C^7), 140.54 (C^5), 141.1 (C^6), 149.14($C^{2''}$), 156.00 q (1C, ^2J 36.3 Hz, $COCF_3$), 158.44 q (1C, ^2J 30.7 Hz, COOH). ^{19}F NMR spectrum (376 MHz, DMSO-d_6), δ, ppm: — 73.50, — 74.12. ^{15}N NMR spectrum (61 MHz, DMSO-d_6), δ, ppm: 126.9 ($N^{1''}$, $N^{3''}$), 218.6 (N^1, $N^{3'}$), 301.6 ($N^{2'}$). MS, m/z (I_{rel},%): 461 (M^+, 20), 369 (11), 131 (100).

4-(4-(2-((2-methyl-1*H*-indol-3-yl) methylene) — 1-(2,2,2-trifluoroacetyl) hydrazinyl)phenyl) — 1,4-dihydroquinazolinium-3 2, 2,2-trifluoroacetate (6b). Yield 55%, m.p. 121–122 °C. ^1H NMR spectrum (600 MHz, DMSO-d_6), δ, ppm: 2.21 s (3H, CH_3), 6.28 s (1H, $H^{4''}$), 7.11 d (1H, CH_{ar}), 7.24 m (2H, CH_{ar}), 7.38 t (1H, *J* 7.7 Hz, CH_{ar}), 7.44 s (5H, $4CH_{ind,}$ CH_{ar}), 7.63 s (3H, CH_{ar}), 7.64 s (1H, $H^{1'}$), 8.57 s (1H, $H^{2''}$), 11.03 m (2H, NH), 12.37 br.s (1H, COOH). 13C NMR spectrum (151 MHz, DMSO-d_6), δ, ppm: 11.34 (CH_3), 55.96 ($C^{4''}$), 115.33 q (1C, *J* 147.38 Hz, CF_3), 118.06 ($C^{8''}$), 119.17 (C^3), 123.08 ($C^{6'}$), 124.11 (C^{4a}), 124.53 (C^7), 127.50 ($C^{6''}$), 127.67 ($C^{7'}$), 127.74 ($C^{5'}$), 127.78 ($C^{5''}$), 127.95 ($C^{7''}$), 129.85 (C^{8a}), 130.97 (C^4), 132.86 (C^{7a}), 136.05 (C^{3a}), 138.50 ($C^{4'}$), 138.87 (C^7), 138.87 (C^5), 144.98 (C^6), 146.48 ($C^{2''}$), 155.30 q (1C, *J* 36.5 Hz, $COCF_3$), 158.17 q (1C, ^2J 30.9 Hz, COOH). ^{19}F NMR spectrum (376 MHz, DMSO-d_6), δ, ppm: — 73.72, — 74.07. MS, m/z (I_{rel},%): 475 (M^+, 27), 345(25), 131 (100).

*General procedure for the synthesis of compounds **7a,b***

0.3 Mmol of corresponding hydrazone **3d,e** was heated in TFA for 45–50 h. The solvent was removed under reduced pressure. The solid residue was treated with water (2.0 ml) and ammonia solution (15%) to adjust pH to 7–8. The precipitate was filtered off and washed with water (2.0 ml). The resulting product **7a,b** was analytically pure and no additional purification was required.

2,2,2-Trifluoro-N' — [(1H-indolyl-3) methylene] — N-phenylacetylhydrazide (7a). Yield 55%, m.p. 154–155 °C. ^1H NMR spectrum (600 MHz, DMSO-d_6), δ, ppm: 7.34 t.t (1H, *J* 7.5, 1.0 Hz, H_p), 7.39 m (1H, H^6), 7.43–7.46 m (2H, H^5, H^6), 7.54 d.d (2H, *J* 8.6, 7.5 Hz, H_m), 7.70 m (1H, H^4), 7.85 d.d (2H, *J* 8.6, 1.0 Hz, H_z, H_o), 7.97 s (1H, $H^{1'}$), 8.78 s (1H, H^2), 11.15 s (1H, N^1H). 13C NMR spectrum (151 MHz, DMSO-d_6), δ, ppm: 116.08 q (CF_3, *J* 288.6 Hz), 118.22 (C_o), 120.64 (C^3), 126.19 (C^2), 126.49 (C_p), 127.57 (C^6), 128.18 (C^5), 128.18 (C^7), 129.08 (C^4), 129.64 (C_m), 131.36 (C^{7a}), 139.39 (C_i), 139.7 ($C^{1'}$), 155.52 q (C=O, *J* 36.2 Hz). ^{19}F NMR spectrum (376 MHz, DMSO-d_6), δ, ppm: 74,52 (s, CF_3). MS, m/z (I_{rel},%): 331 (M^+, 100), 262 (44).

2,2,2-Trifluoro-N' — [(2-methyl-1H--indolyl-3)methylene] — N-phenylacetylhydrazide (7b). Yield 64%, m.p. 164–165 °C. ^1H NMR spectrum (500 MHz, DMSO-d_6), δ, ppm: 2.21 s (3H, CH_3), 7.43–7.47 m (5H, H^4, H^5, H^6, H^7 and H_p), 7.52 d.d (2H, *J* 8.5, 1.4 Hz, H_o), 7.57 d.d (2H, *J* 8.5, 7.2 Hz, H_m), 7.63 s (1H, $H^{1'}$), 10.99 s (1H, N^1H). ^{13}C NMR spectrum (151 MHz, DMSO-d_6), δ, ppm: 115.98 q (CF_3, *J* 288.8 Hz), 118.04 (C^3), 124.4

(C_o), 127.49 (C^6), 127.67 (C_p), 127.76 (C^5), 127.78 (C^7), 129.27 (C_m), 130.99 (C^4), 136.06 (C^2), 132.84 (C^{7a}), 139.22 ($C^{1'}$), 139.44 (C_i), 155.28 q (C=O, *J* 36.2 Hz). ^{19}F NMR spectrum (376 MHz, DMSO-d_6), δ, ppm: — 74,45 (s, CF_3). MS, m/z (I_{rel},%): 345 ($M^{+\cdot}$ 80), 276 (100).

Results and discussion

Arylhydrazones of indole-3-carbaldehydes **3a-e**, which were obtained by heating indole-3-carbaldehydes **1a,b** with phenylhydrazines **2a-d** in ethanol with the addition of HCl, were used as C-nucleophiles for the studies (Scheme 1). It is known that the *E*-configuration of the C=N bond is more thermodynamically favorable for arylhydrazones. This was confirmed by the data of X-ray structural analysis [15, 16].

We previously described that heating of quinazoline 4 with hydrazones **3a-c** in TFA resulted in the formation of products **5a-c** (Scheme 2) [14].

In current work, we have found that hydrazones **3d,e**, which do not contain substituents in the phenyl fragment of the molecule, are added to quinazoline **4** at the $C^{7'}$ atom.

The reaction of quinazoline **4** with hydrazones **3d,e** in TFA yielded adducts **6a,b** (Scheme 3).

The mass spectra of compounds **6** contain molecular ions corresponding to the addition products of hydrazones **3d,e** to quinazoline **4**. The mass spectra of compounds 6 contain molecular ions corresponding to the addition products of hydrazone to quinazoline. The ^{1}H NMR

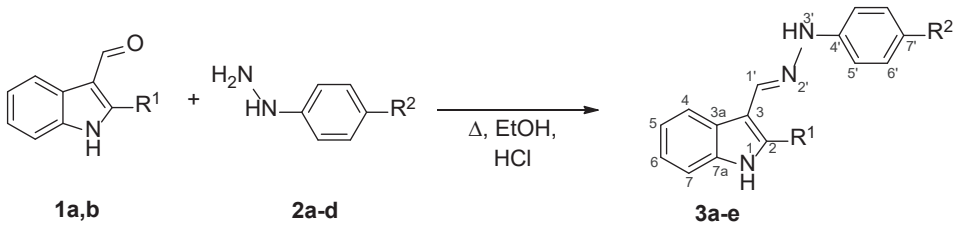

1:
a: R^1 = H
b: R^1 = Me

2:
a: R^2 = NO_2
b: R^2 = Me
c: R^2 = F
d: R^2 = H

3:
a: R^1 = Me; R^2 = NO^2
b: R^1 = Me; R^2 = Me
c: R^1 = Me; R^2 = F
d: R^1 = H; R^2 = H
e: R^1 = Me; R^2 = H

Scheme 1

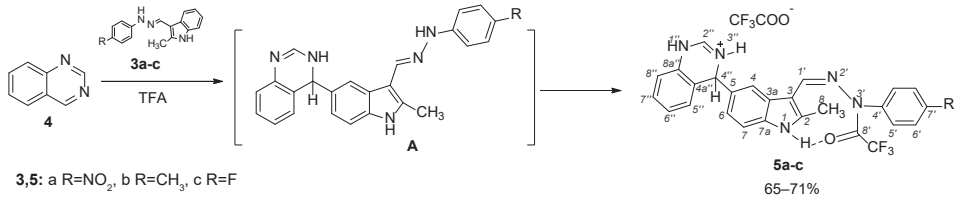

3,5: a R=NO_2, b R=CH_3, c R=F

Scheme 2

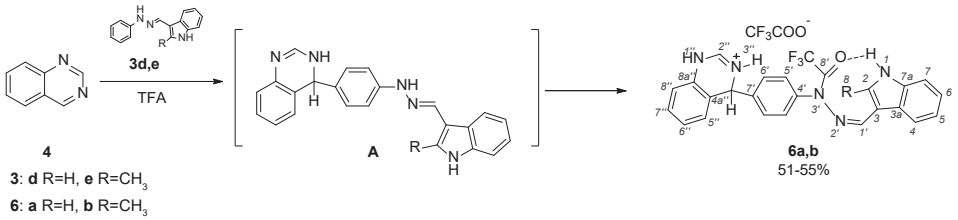

Scheme 3

spectrum contain characteristic signals: the H4" proton singlet at 6.24 ppm (**6a**) and a pair of two-proton doublets of aromatic protons $H^{6'}$, $H^{5'}$ (7.61 and 7.92 ppm, respectively (**6a**)). These data confirm the addition of hydrazones **3d,e** to compound **4** by the *p*-position of the phenyl group. Since the signal of the NH-proton of the indole fragment is retained in adducts **6**, it is obvious that the hydrazine part of the molecule undergoes acylation.

It should be noted that the 2D ^{1}H-^{13}C gHMBC spectra of adducts **6a,b** contain intense cross peaks between the characteristic quartet of **C8'** atom in the trifluoroacetyl group, in particular, at 155.9 ppm for compound 6a ($^{2}J_{C\text{-}F}$ = 36.3 Hz), and the broadened signal of the $N^{1}H$ proton (see Fig. 1), indicating the presence of an intramolecular hydrogen bond N-H…O=C. Due to the presence of an intramolecular hydrogen bond in the molecule, it can be assumed that the C=N bond of compounds **6a,b** in DMSO-d_6 has the *Z*-configuration, as in adducts **5**.

We suggest that the formation of trifluoroacetyl derivatives of quinazoline **6**, as well as adducts **5**, occurs in several stages. Initially, the addition of hydrazone to quinazoline takes place, followed by acylation of the adduct with TFA at the $N^{3'}H$-group with the formation of compounds **6**.

Since acylation of the NH group occurred during the C,C-coupling described above, we assumed that the same reaction would take place upon heating hydrazones **3** in TFA in the absence of quinazoline. This was confirmed in the course of experiments and hydrazides **7** were obtained (Sheme 4).

The structure of acylation products **7a,b** was confirmed by ^{1}H, ^{13}C, ^{15}N, and

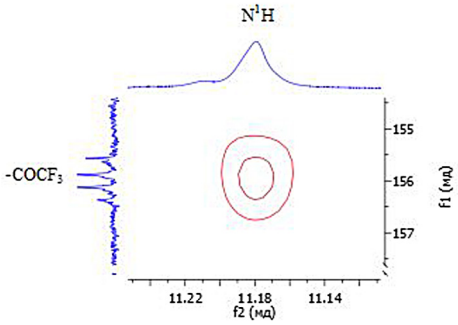

Fig. 1. Fragment of the NMR 2D ^{1}H-^{13}C HMBC spectrum for compound **6a**

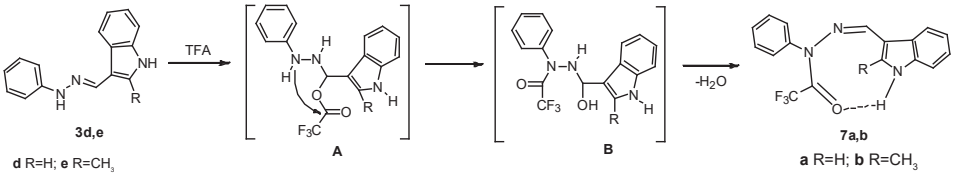

Scheme 4

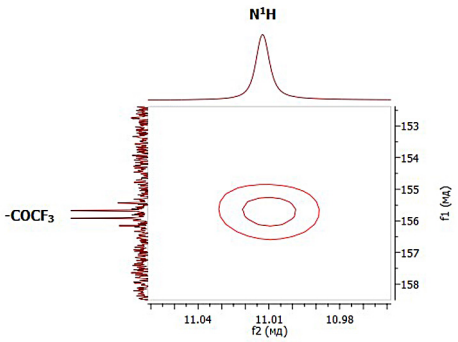

Fig. 2. Fragment of the NMR 2D 1H-13C HMBC spectrum for compound **7**

^{19}F NMR spectroscopy including 2D ^{1}H-^{13}C HSQC / HMBC correlation experiments. Due to the fact, that the spectra of compounds **7a,b** contain signals of the NH-protons of the indole fragment, it is obvious that the hydrazine part of the molecule undergoes acylation. 2D ^{1}H-^{13}C HMBC spectra of compounds **7a,b** contain characteristic intense cross-peaks between the carbon quartet of the trifluoroacetyl group (155.4 ppm, $^{2}J_{C\text{-}F}$ = 36.7 Hz) and the N^{1}H proton of the indole fragment (11.01 ppm). We believe that these cross peaks are due to the spin-spin interaction through the hydrogen bond (see Fig. 2).

It should be mentioned that the obtained hydrazides **7** do not react with quinazoline **4**. Heating of quinazoline **4** with hydrazides **7a, b** in TFA gave the starting compounds **7**. The inertness of hydrazides **7** in the studied reactions of C,C-coupling confirms that the first stage of the multistep reaction is precisely the addition of the hydrazone **3** to the quinazoline **4**, and then the stage of acylation with acid occurs.

Conclusions

As a result of this work, it was found that the reactions of indole-3-carbaldehyde arylhydrazones with quinazoline can proceed either at 5- or 7' — position of the arylhydrazone molecule. It was shown that in the absence of substituents at both positions, the C^{7} atom is the most active nucleophilic center.

Acknowledgements

The authors are grateful to the Russian Foundation for Basic Research (grant 18-33-00727 mol_a) for financial support of the research.

References

1. D'yakonov AL, Telezhenetskaya MV. Quinazoline alkaloids in nature. Chem. Nat. Compd. 1997;33:221–267.
   DOI: 10.1007/BF02234869
2. Aniszewski T. Alkaloids (Second Edition). Helsinki: Elsevier Science, 2015. 496 p.
3. Asif M. Chemical Characteristics, Synthetic Methods, and Biological Potential of Quinazoline and Quinazolinone Derivatives. Int. J. Med. Chem. 2014;ID 395637:1–27.
   DOI: 10.1155/2014/395637
4. Solyanik GI. Quinazoline compounds for antitumor treatment. Exp. Oncology. 2019;41:3–6.
   DOI: 10.32471/exp-oncology.2312–8852.vol-41-no-1.12414
5. Tregubenko IP, Tarakhtii EA, Chibiriak MV, Golomolzin BV, Egorova LG. K voprosu o mekhanizme deystviya dialkilaminoetiltiol'nykh proizvodnykh pirimidina

i khinazolina. Radiobiologiia. 1984;24:838–846. Russian. Available from: https://elibrary.ru/item.asp?id=25627353
6. Pilicheva TL, Chupakhin ON, Postovsky IYa. Addition of nucleophiles to 3-methylquinazolinium iodide. Chem. Het. Comp. 1975;11:496–499.
DOI: 10.1007/BF00502444
7. Azev YuA, Shorshnev SV, Golomolzin BV. Specific features of the reactions of quinazoline and its 4-hydroxy and 4-chloro substituted derivatives with C-nucleophiles. Tetr. Lett. 2009;50:2899–2903.
DOI: 10.1016/j.tetlet.2009.03.199
8. Azev YuA, Koptyaeva OS, Seliverstova EA, Ivoilova AV, Pospelova TA. Synthesis of Stable σ-Adducts by Arylation of Quinazoline. Rus. J. Gen. Chem. 2019;89(12):2374–2377.
DOI: 10.1134/S1070363219120089
9. Sundberg RJ. Indoles. San Diego: Academic Press Inc, 1996. 175 p.
10. Chadra N, Silakari O. Key Heterocycle Cores for Designing multitargeting molecules. Patiala: Elsevier, 2018, 285 p.
DOI: 10.1016/B978-0-08-102083-8.00008-X
11. Anastas PT, Warner JC. Green Chemistry Theory and Practice. New York: Oxford University Press, 1998, 516 p.
12. Charushin VN, Chupakhin ON. Topics in Heterocyclic Chemistry: Metal-free C-H functionalization of aromatic compounds through the action of nucleophilic reagents. Eds.: Charushin VN, Chupakhin ON. Switzerland: Springer; 2014;37:1–50.
13. Makosza M, Wojciechowski K. Topics in Heterocyclic Chemistry: Nucleophilic Substitution of Hydrogen in Arenes and Heteroarenes. Eds.: Charushin VN, Chupakhin ON. Switzerland: Springer; 2014;37:51–105.
14. Azev YuA, Koptyaeva OS, Eltzov OS, Yakovleva YuA, Pospelova TA, Bakulev VA. Quinazoline addition to indole hydrazone derivatives in TFA as a facile synthesis of trifluoroacetylhydrazide quinazoline σ-adducts. Mend. Comm. 2020;30:226–227.
DOI: 10.1016/j.mencom.2020.03.032
15. Zabaleta N, Uria U, Reyes E, Carrillo L, Vicario JL. Ion-pairing catalysis in the enantioselective addition of hydrazones to N-acyldihydropyrrole derivatives. Chem. Comm. 2018;54:8905–8908.
DOI: 10.1039/C8CC05311A
16. Tung T, Tezcan H, San M, Bueykguengoer O, Yagbasan R. N-(4-Nitrobenzylidene) — N'-phenylhydrazine. Acta Cryst., Sec. C. 2003;59:528–529.
DOI: 10.1107/S0108270103016019

Chimica Techno Acta. 2020. Vol. 7, no. 3. P. 116–127.
ISSN 2409–5613

DOI: 10.15826/chimtech.2020.7.3.04

E. A. Mikhnevich,[a*] A. P. Safronov,[ab] I. V. Beketov,[ab] A. I. Medvedev[ab]

[a] *Ural Federal University, 620002, 19 Mira St., Ekaterinburg, Russia*
[b] *Institute of Electrophysics UB RAS, 620016, 106 Amundsen St., Ekaterinburg, Russia*
**email: emikhnevich93@gmail.com*

Carbon coated Nickel Nanoparticles in Polyacrylamide Ferrogels: Interaction with Polymeric Network and Impact on Swelling

Polyacrylamide ferrogels with embedded magnetic nanoparticles of metallic nickel (Ni) and nanoparticles of nickel coated with a carbon shell (Ni@C) were synthesized by radical polymerization in water. The effect of the carbon shell on the interaction of Ni and Ni@C nanoparticles with polyacrylamide matrix and on swelling ratio of the ferrogels has been studied. The deposition of carbon on the surface of Ni nanoparticles worsens their interaction with polyacrylamide but at the same time elevates the water uptake by ferrogels.

Keywords: nanoparticles; nickel; composites; ferrogels; polyacrylamide; carbon coatings.

Received: 26.08.2020. Accepted: 06.10.2020. Published: 07.10.2020.

1. Introduction

A hydrogel is a three-dimensional polymeric network swollen in water. The internal structure of a hydrogel includes flexible polymeric sub-chains, which are cross-linked in a certain number of points. Due to the internal cross-linking the polymeric network of a hydrogel might be considered as a combined huge molecule. From the thermodynamic point of view hydrogel is a solution of this molecule in water. Despite the fact that it contains large amount of water, hydrogel is not a fluid but an elastic material maintaining its shape. Due to their unique properties such as mechanical elasticity, softness, and biocompatibility, hydrogels have been applied in a variety of fields, including smart devices that respond to stimuli and soft actuators in biomedicine and agriculture [1, 2].

Hydrogels are often functionalized by incorporating various physically, chemically, and biologically active moieties, which endows hydrogels with new functions, such as response to specific external stimuli and increased mechanical stability [3]. Stimulus-responsive hydrogels can markedly change their physical and/or chemical properties when exposed to external triggers (pH, temperature, light, magnetic or electric field) [4]. For instance, the inclusion of magnetic nanoparticles (MNPs) in such a polymer network gives magnetic hydrogels (ferrogels) that react to an external magnetic field [5]. Ferro-

gels are usually obtained by crosslinking hydrophilic monomers in a stabilized aqueous dispersion of magnetic nanoparticles (ferrofluid), which, in turn, provides good dispersion of nanoparticles in a polymer matrix. One of the main advantages of ferrogels over traditional stimulus-responsive polymers is that they can be remotely activated by a non-contact force (magnetic field). This unique property makes ferrogels prospective advanced material in various fields such as drug delivery [6, 7], soft robotics [8], tissue reconstruction [9, 10] and environmental engineering [11, 12].

Huang et al. [9] reported about a hydrogel formed by gelatin and β-cyclodextrin with embedded magnetic Fe_3O_4 nanoparticles for pulsed electromagnetic field therapy. Chondrogenesis of mesenchymal stem cells grown on a magnetic hydrogel was enhanced by a magnetic field. Czichy et al. [13] investigated the mechanical properties of alginate-methylcellulose hydrogels containing magnetite nanoparticles for the use in the additive manufacturing of implants. The study was an introduction to further research on the effect of an external magnetic field on the mechanical stability of composites. The most extensive study on ferrogels was carried out by Zrinyi et al. [14–16] on magnetic silicone elastomers filled with carbonyl iron or micron-sized magnetite. The modulus of elasticity of these magnetoelastic gels was studied in both uniform and inhomogeneous magnetic fields. The influence of the content of magnetic particles and their distribution at various combinations of magnetic field orientation and deformation on the modulus has been systematically studied. Meanwhile, studies of synthetic water-based ferrogels are very limited.

In the literature most of the studies address ferrogels based on polyacrylamide (PAAm) chemically cross-linked polymeric network. Thus, the series of works were performed by the group of Galicia et al [17–19] on ferrogels with embedded maghemite nanoparticles. Maghemite nanoparticles were synthesized using ferrofluid obtained by co-precipitation of iron oxides from Fe^{2+}/Fe^{3+} mixed solutions. Ferrogels had weakly cross-linked polymeric network with monomer-to-cross-linker ratio 1000 and more and contained up to 7% (vol.) of nanoparticles. The structure of ferrogels in the swollen state and the mechanical properties were studied. It was shown that the Young modulus of ferrogels enlarged from 4 to 16 kPa with the increase in nanoparticles content.

In our previous works [20–22] we have studied PAAm ferrogels with embedded iron and nickel nanoparticles, which were synthesized by the high-power pulsed physical dispersion by the electrical explosion of metal wire (EEW) [23]. The magnetostriction in the uniform magnetic field and the compression modulus of ferrogels were characterized. It was shown that ferrogels with iron nanoparticles contract by approximately 9% (vol) in the uniform magnetic field 420 mT applied for 4 hours. Shear modulus of ferrogels with embedded iron nanoparticles increased from 0.5 to 2.5 kPa with the elevation of nanoparticles content up to 4% (vol.) [21]. In PAAm ferrogels with nickel nanoparticles it was shown [22] that the elastic modulus of ferrogels linearly depended on the content of the embedded nickel nanoparticles. The applied magnetic field 270 Oe in the parallel direction to the compression increased the elastic modulus by 10% while the application of the magnetic field in the transverse direction decreased the modulus.

Although ferrogels with embedded metal nanoparticles show a potential for

their use as a smart material in soft sensors and actuators their application in bioengineering and medicine is doubtful due to the toxicity of metallic iron and nickel. To overcome this shortcoming the surface of metallic particles should be covered with a biocompatible layer, which prevents the contact of an open metallic surface with biological liquids. It our earlier report [24] it was shown that the surface of nickel nanoparticles produced via EEW can be modified by the in-situ carbon deposition. Such a deposition is provided by adding volatile hydrocarbons to the working gas of EEW unit. In the process of the electrical explosion hydrocarbon molecules decompose to elements and carbon deposits on the surface of condensing metal nanoparticles.

The modification of the surface of nickel nanoparticles opens a question on how would it influence the properties of ferrogels with embedded metal nanoparticles. In the present study we aimed to clarify two aspects of this possible influence. First, we will focus on the interfacial interaction between polyacrylamide and modified nickel nanoparticles. Second, we will address the influence of the carbon deposition on the volume swelling of ferrogels, which is a basic property for their performance in sensors and actuators.

2. Experimental Part

2.1. Synthesis of MNPs, composites, and ferrogels

Nickel magnetic nanoparticles (Ni MNPs) were synthesized by the electrical explosion of wire (EEW). The essence of EEW is the evaporation of a metal wire by a high-voltage electrical discharge in an inert atmosphere of argon and the subsequent condensation of metal vapors into spherical nanoparticles. Nickel nanoparticles coated with a carbon shell (Ni@C MNPs) were synthesized using a mixture of argon with the addition of butane as a working gas of EEW unit. Carbon content in the Ni@C was 2% (wt.). The thickness of the carbon shell was 4–6 nm. The carbon was in an amorphous state. The details of the synthetic procedure can be found in our previous reports [25].

The MNPs composites for microcalorimetry studies were prepared in the entire range of weight fraction of MNPs. Linear polyacrylamide (PAAm) was synthesized by free radical polymerization in 1.6 M water solution. Hydrogen peroxide in 18 mM concentration was an initiator of the reaction. Polymerization was done at two steps: first at 60 °C for 30 min, second at 100 °C for 60 min. Molecular weight of linear PAAm was $7.3 \cdot 10^5$ as determined by viscometry of water solution at 25 °C. The stock solution of PAAm was then vigorously stirred with weighted amounts of Ni and Ni@C MNPs in proportions to get resulted composites with certain MNPs/PAAm ratio. The suspension of MNPs in PAAm solution was homogenized by ultra-sound treatment and then cast upon Teflon plate and dried to the constant weight at 70 °C. The obtained films of NP/PAAm composites were then used for the microcalorimetry measurements of the enthalpy of dissolution in distilled water.

Ferrogels were synthesized by radical polymerization of acrylamide (AA) (Panreac Quimica SA) of in 1.6 M water solution. Methylene diacrylamide (MDAA) (MERCK) was a cross-linker in a molar ratio to monomer of 1:100. Ammonium persulfate (APS) was used as the initiator of the polymerization. Magnetic Ni/Ni@C

nanoparticles were added to the reaction mixture in portions of a weighed 20% water-based suspension stabilized with Dispex A40 dispersant (R. T. Vanderbilt). The suspension was homogenized in an ultrasonic bath for 20 minutes. Polymerization was carried out for 60 minutes at 80 °C. Synthesized ferrogels were washed in distilled water for two weeks with daily water renewal to remove residual impurities. The equilibrium swelling ratio (maximum water uptake) was determined as the ratio of the water content in the gel to the weight of the dry gel by weighing the swollen sample of the gel and the dry residue after drying to a constant weight at 70 °C.

2.2. Methods

Transmission electron microscopy (TEM) was performed using a JEOL JEM2100 microscope operated at 200 kV. The specific surface area of MNPs was measured via low temperature adsorption of nitrogen (Brunauer-Emmett-Teller approach) using a Micromeritics TriStar3000 analyzer. Phase composition of MNPs was examined using an X-ray diffractometer Bruker D8 Discover operated at Cu Kα radiation (wavelength λ = 1.5418 A) with a graphite monochromator and a scintillation detector. XRD results were processed using the built-in Bruker software TOPAS-3 provided the Rietveld full-profile refinement. Magnetic hysteresis loops were measured using a vibrating sample magnetometer (Cryogenics). Calorimetric measurements were done at 25 °C using a Calvet differential microcalorimeter of laboratory design. The sensitivity was 31.5 mV/W, cell volume was 10 cm^3. The stability of a baseline was ±0.5 μV. Enthalpies of dissolution of PAAm/Ni, PAAm/Ni@C, and PAAm/C composites in water were measured using glass ampoule cells. Water was placed in a stainless steel cell and small portion of a composite film (approximately 10–30 mg by weight) was put into a thin-walled glass ampoule. This specimen was dried to a constant weight in vacuum and then the ampoule was sealed. A sealed ampoule was placed in the cell with water in it. After thermal equilibration until the baseline of calorimeter kept at a constant level the ampoule was broken inside the cell and the heat effect of the dissolution of a composite in water was measured. The absolute values of measured heat effects of dissolution were from 0.5 to 2 Joule depended on the composition of a composite. The absolute error of calorimetric measurements was 0.05 Joule.

3. Results and discussion

3.1. Characterization of Ni and Ni@C MNPs

Fig. 1 shows the transmission electron microscopy (TEM) images of Ni and Ni@C MNPs. Both batches of MNPs contain individual spherical particles. A typical diameter of spherical Ni MNPs (Fig. 1a) lay within 10–100 nm range. Deposited thin carbon layers are clearly observed on the surface of Ni@C nanoparticles (Fig. 1b).

The average diameter of MNPs was estimated based on the value of the specific surface area of MNPs, which was determined by low-temperature nitrogen adsorption. The specific surface area of Ni and Ni@C MNPs obtained from the isotherms of nitrogen adsorption by the Brunauer-Emmett-Teller (BET) treatment were equal to 12.6 and 10.8 m^2/g respectively. Straightforward geometrical consideration of the surface of a sphere related to its

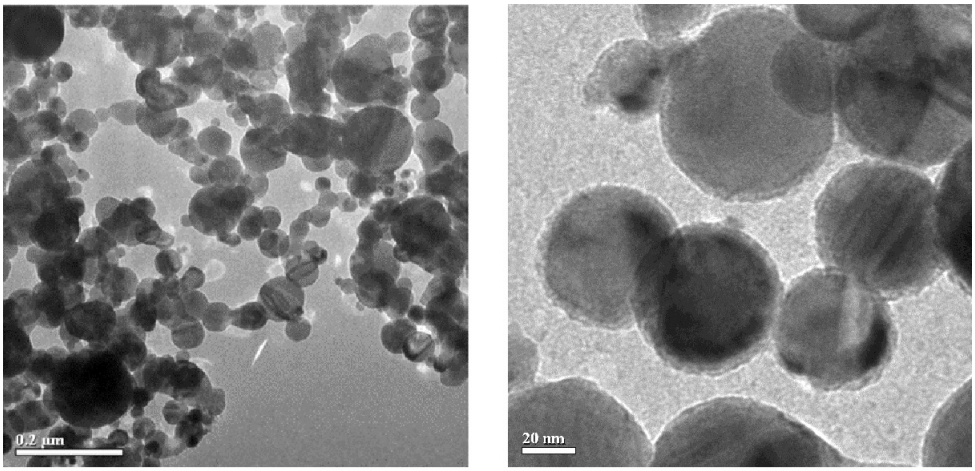

(a) (b)

Fig. 1. TEM images of Ni (a) and Ni@C (b) MNPs.

mass gives the following simple equation for the diameter (d) of the sphere in relation to its surface (S) and the density (ρ) of its material:

$$d = \frac{6}{S\rho} \quad (1)$$

If applied to the specific surface area of the MNPs in air-dry powder equation (1) gives the average value of the diameter for the ensemble of MNPs. If S is in m^2/g and ρ is in g/cm^3 equation (1) yields the average diameter in micron. Calculated values for Ni and Ni@C MNPs are presented in Table 1. The average diameters are close to each other. The average diameter of Ni@C nanoparticles is little higher than that for Ni nanoparticles. It is consistent with the presence of a deposited carbon layer on the surface of Ni@C nanoparticles.

The phase composition of Ni and Ni@C MNPs was characterized by X-ray diffraction (XRD). According to X-ray powder diffraction data (Fig. 2), the Ni sample contained 100% α-Ni phase with a cubic face-centered lattice; the unit cell parameter a = 0.3523(2) nm. XRD pattern for Ni@C MNPs also revealed 100% α-Ni phase with

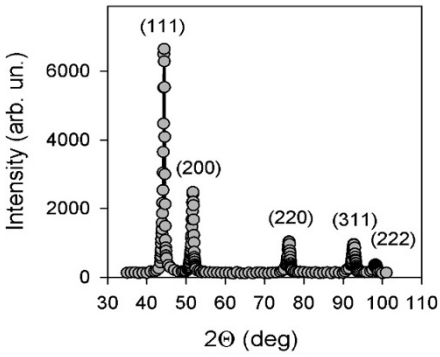

Fig. 2. XRD pattern of Ni MNPs

Table 1

Characteristics of magnetic fillers

MNPs	Density, g/cm^3	Shape	S_{sp}, m^2/g	d_{av}, nm	*M_s, kA/m	**H_c, kA/m
Ni	8.9	spherical	12.6	58	454	20.7
Ni@C	8.9	spherical	10.8	62	339	7.7

* — saturation magnetization; ** — coercive force

the unit cell parameter a = 0.3533(3) nm. Carbon layer was not detected in XRD pattern for Ni@C because the deposited layer was too thin and its content (2%) was below the sensitivity of XRD.

Fig. 3. Shows magnetic hysteresis loops for Ni and Ni@C MNPs. In both cases magnetization reached saturation in high field range. The parameters of magnetic hysteresis loops — saturation magnetization and coercive force are given in Table 2. According to these data, Ni and Ni@C powders were soft magnetic materials with low coercive force. Saturation magnetization of Ni@C nanoparticles was by approximately 25% lower than saturation magnetization of Ni MNPs. It was likely due to the distortions of the crystalline lattice in the surface layer of Ni@C particles under the influence of deposited carbon, which could happen because of limited dissolution of carbon in the lattice.

The structural characterization of Ni and Ni@C MNPs showed that these nanoparticles are very much alike despite the existence of the deposited carbon layer on the surface of Ni@C MNPs. Meanwhile, this factor was of decisive importance for the interfacial properties of polymeric composites with Ni and Ni@C MNPs.

3.2. Interfacial adhesion of PAAm to MNPs

The basic thermodynamic property, which stands for the interaction of a polymeric chain of composite with an embedded solid particle, is the enthalpy of interfacial adhesion. The latter is the enthalpy change during the adsorption of a macromolecule on a solid surface. This process establishes adhesive contacts at the interface between a macromolecule and a particle due to molecular interactions. Such enthalpy change cannot be measured directly in calorimetric experiment as Ni, Ni@C, and PAAm are solids. The enthalpy of interfacial adhesion was determined using an appropriate thermochemical cycle (Hess cycle), which included quantities measurable in calorimeter. In case of polymeric composites with embedded solid particles the enthalpy of interfacial adhesion is equal to the enthalpy of composite mixing. Since the solid particles have not dissolved in a polymeric matrix, the only source of enthalpy change is the interface interaction. The Hess cycle for the enthalpy of mixing of PAAm/Ni (or PAAm/Ni@C) composite constitutes the combination of the following processes.

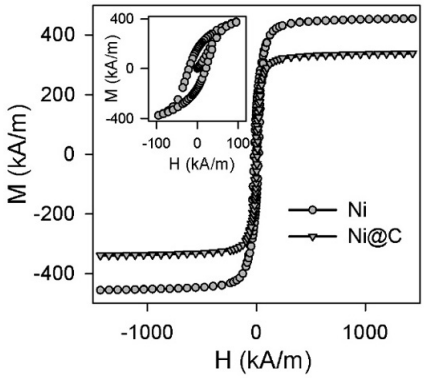

Fig. 3. Magnetic hysteresis loops for Ni and Ni@C MNPs. Inset — hysteresis loop in low field range for Ni MNPs

1) PAAm + Ni MNPs = Composite PAAm/Ni + ΔH_{adh}

2) PAAm + water (excess) = PAAm solution + $\Delta H_{dis,p}$

3) Ni MNPs + water (excess) = Ni MNPs suspension + ΔH_{wet}

4) PAAm solution + Ni MNPs suspension = Ni MNPs suspension in PAAm solution + ΔH_{mix}

5) Composite PAAm/Ni + water (excess) = Ni MNPs suspension in PAAm solution + $\Delta H_{dis,c}$

The combination of these steps gives for the enthalpy of adhesion:

$$\Delta H_{adh} = \omega_{PAAm}\Delta H_{dis,p} + \omega_{Ni}\Delta H_{wet} + \\ + \Delta H_{mix} - \Delta H_{dis,c} \quad (2)$$

In Equation (2) ω_{PAAm} and ω_{Ni} are weight fractions of PAAm and Ni in a composite; $\Delta H_{dis,p}$ is the enthalpy of dissolution of PAAm in water; ΔH_{wet} is the enthalpy of wetting of air-dry Ni MNPs in water; ΔH_{mix} is the enthalpy of mixing of PAAm water solution with Ni MNPs water suspension; $\Delta H_{dis,c}$ is the enthalpy of dissolution in water for a composite with ω_{PAAm} and ω_{Ni} composition.

Fig. 4 (a) shows dependencies of the enthalpy of dissolution in water versus the weight content of embedded particles for PAAm composites. Together with PAAm/Ni and PAAm/Ni@C composites we also took as a reference PAAm/Carbon composite which was prepared using commercial sample of carbon black with specific surface area 124 m^2/g. The value at the left-hand vertical axis corresponds to the enthalpy of dissolution of PAAm in water, which is $\Delta H_{dis,p}$. The value at the right-hand axis corresponds to the enthalpy of wetting of air-dry particles, which is ΔH_{wet}. The symbols at the field of the plot corresponds to $\Delta H_{dis,c}$ values for the composites with certain fractions of PAAm and a filler.

One can notice that the dependence of $\Delta H_{dis,c}$ for PAAm/Ni composites is convex upward, while the dependencies of $\Delta H_{dis,c}$ for PAAm/Ni@C and PAAm/Carbon are concave downwards. The data presented in Fig. 4 (a) were used to calculate the enthalpy of interfacial adhesion in composites ΔH_{adh} using equation (2). It is worth noting that the values of ΔH_{mix} (step (4) of the Hess cycle) typically can be neglected as they lay within the experimental error of the other quantities of Hess cycle.

The dependence of the enthalpy of interfacial adhesion versus the content of solid particles in PAAm composites is shown in Fig. 4 (b). There is a substantial difference between dependencies of the enthalpy of adhesion for PAAm/Ni and PAAm/Ni@C composites. In case of PAAm/Ni composite the enthalpy of adhesion is negative over the entire composition range. It

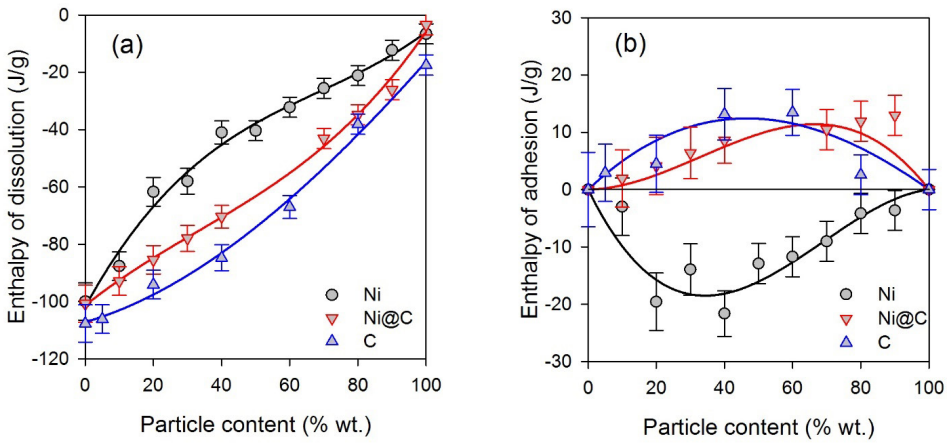

Fig. 4. a) — Concentration dependence of the enthalpy of dissolution of PAAm composites with embedded Ni, Ni@C, and C particles; b) — Concentration dependence of the enthalpy of interfacial adhesion in PAAm composites with embedded Ni, Ni@C, and C particles

means that the adhesion contact between PAAm chain and the surface of Ni MNP is energetically favorable. Such interaction promotes adsorption of PAAm chains on the surface of Ni MNPs.

On the contrary, in case of PAAm/Ni@C composite the enthalpy of adhesion is positive over the entire composition range. It means that PAAm chains do not interact with the surface of Ni@C MNPs. No doubts that such interaction is energetically unfavorable the deposited carbon layer on the surface of MNPs. The results for the reference system PAAm/Carbon clearly confirm this fact. In the PAAm/Carbon composites the enthalpy of adhesion is also positive over the entire composition range similar to the case of PAAm/Ni@C composites.

Thus, the obtained thermochemical data showed that the deposition of carbon on the surface of Ni MNPs worsened the adhesion of PAAm chains to modified Ni MNPs.

3.3. Swelling of PAAm ferrogels with Ni and Ni@C

Fig. 5 (a) shows the dependence of the relative degree of swelling of PAAm/Ni and PAAm/Ni@C ferrogels versus the weight fraction of MNPs in ferrogel. The relative degree of swelling is the swelling ratio (water uptake) of a ferrogel divided by the swelling ratio of a blank PAAm gel with the same composition. The data presented in Fig. 7 (a) refer to gels with a network density of 100 monomer units in linear sub-chains per one cross-link. It is worth noting that the relative swelling decreases with MNPs content in the case of ferrogels with Ni MNPs, and it increases in the case of ferrogels with Ni@C MNPs.

The same trend is shown in Fig. 5 (b), which presents the swelling ratio of ferrogels with different network density containing the 3.1% (wt.) of MNPs. Both in the case of ferrogels with Ni MNPs and in the case of ferrogels with Ni@C MNPs the swelling ratio increases if the network density of a gel decreases. It is a general trend in gels. If a number of monomer

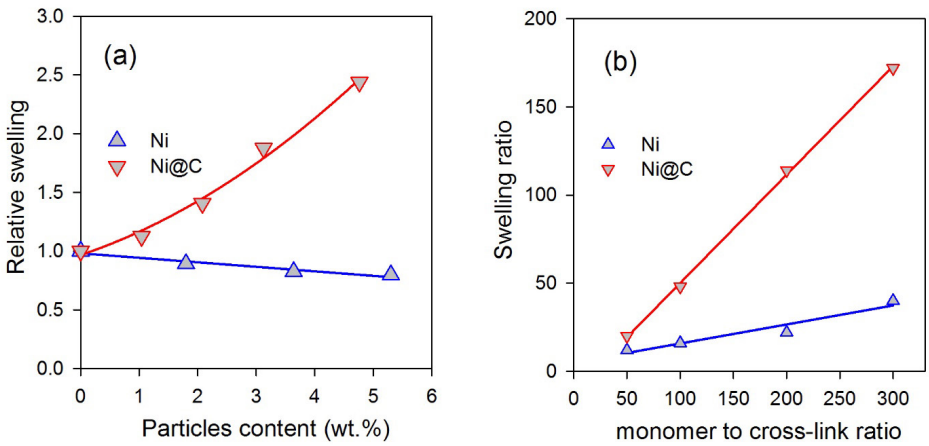

Fig. 5. a) — Dependence of the relative degree of swelling of PAAm ferrogels with Ni and Ni@C MNPs with respect to the unfilled gel matrix (monomer to cross-link ratio 100:1); b) — Dependence of the swelling ratio of PAAm ferrogels with Ni and Ni@C MNPs on the length of the linear sub-chains between the crosslinks (MNPs content 3.1%)

units in linear sub-chains enlarge and the number of cross-links diminishes, then the network loosens and it can absorb more water. Thus the water uptake of a gel increases. Although the basic trend in the dependence of the swelling ratio on the network density is the same for both types of ferrogels, there is s remarkable difference in the absolute values of the swelling ratio. It is much higher in the case of Ni@C ferrogels. In ferrogels with the lowest network density (300 monomer units per one cross-link) the swelling ratio of PAAm ferrogel with embedded 3% Ni@C MNPs is four times larger than that for the ferrogel with the same composition but with embedded Ni MNPs.

The reason for such a difference in swelling of ferrogels with embedded Ni or Ni@C MNPs apparently stems from the different adhesion of PAAm chains to the surface of particles. PAAm ferrogels differ from PAAm composites, because ferrogels contain water besides polymer and MNPs. Nevertheless, interaction between PAAm chains and the surface of MNPs governs the swelling of ferrogel. If interaction between polymeric chains and MNPs is strong, then the PAAm sub-chains in the network are adsorbing on the surface of the particles. Adsorption of chains effectively increases the networking density and diminishes the water uptake of the gel matrix. It is the case of PAAm ferrogel with enbedded Ni MNPs.

In turn, if PAAm chains do not interact with the surface of MNPs, then the MNPs will effectively repel the sub-chains of the networks. It will increase the mobility of the network, and it will promote extra swelling of ferrogel. It is the case of PAAm ferrogel with embedded Ni@C MNPs.

4. Conclusions

Metallic magnetic nanoparticles (MNPs) are prospective for the use in smart soft materials suitable for bioengineering and medical applications. However, to provide biocompatibility they need to be coated with protective layers. Deposited carbon coating is among them. Meanwhile, deposition of carbon affects functional properties of MNPs and materials, in which they are embedded. In the present study the interfacial interaction of carbon coated Ni MNPs (Ni@C) with polyacrylamide (PAAm) has been studied in comparison with Ni MNPs focusing on application in PAAm ferrogels. The interfacial adhesion of PAAm chains to the surface of MNPs was studied by means of thermochemical cycle based on calorimetric measurements of the enthalpy of dissolution of PAAm/Ni and PAAm/Ni@C composites in water, and the enthalpy of adhesion to the surface of MNps was determined in the entire range of MNPs content in the composite. It turned out that while interaction of Ni MNPs with PAAm was energetically favorable and led to the evolution of heat (negative enthalpy change) during adhesion, deposited carbon layer provided poor interaction of PAAm with the surface of Ni@C MNPs. The enthalpy of interaction between PAAm and Ni@C MNPs was positive over the entire range of MNPs content. It means that PAAm do not interact with the surface coated with carbon layer. It provided a marked impact on the swelling ratio (water uptake) of PAAm ferrogels with embedded Ni@C MNPs in comparison with ferrogels with embedded Ni MNPs. The swelling ratio of PAAm gel matrix diminished with the embedding of Ni MNPs due to the adsorption of PAAm sub-chains on the sur-

face of MNPs. On the contrary, the embedding of Ni@C MNPs in PAAm gel matrix resulted in the increase of its swelling ratio owing to the effective repelling of PAAm chains by the carbon layer on the surface of MNPs. It means that poor interaction at the interface not necessarily worsens the functional properties of soft biocompatible materials. The increase of the swelling ratio might be an advantageous feature in certain applications of ferrogels in biocompatible sensors and actuators. In a whole, obtained results showed that coating of the surface of MNPs not only provides biocompatibility of MNPs but might as well be a versatile tool to modify the functional properties of smart materials based on nanoparticles.

Acknowledgements

The study was financially supported by RFBR, project number 19-38-90229.

References

1. Abasi S, Podstawczyk DA, Sherback AF, Guiseppi-Elie A. Biotechnical properties of poly(HEMA- co-HPMA) hydrogels are governed by distribution among water states. ACS Biomater. Sci. Eng. 2019;5(10):4994–5004.
   DOI: 10.1021/acsbiomaterials.9b00705
2. Chen Z, Zhao D, Liu B, Nian G, Li X, Yin J, Qu S, Yang W. 3D printing of multifunctional hydrogels. Adv. Funct. Mater. 2019;29(20)1–8. doi:10.1002/adfm.201900971
3. Zhang YS, Khademhosseini A. Advances in engineering hydrogels. Science. 2017;356(6337):eaaf3627.
   DOI: 10.1126/science.aaf3627
4. Lui YS., Sow WT., Tan LP., Wu Y., Lai Y., Li H. 4D printing and stimuli-responsive materials in biomedical aspects. Acta Biomater. 2019;92:19–36.
   DOI: 10.1016/j.actbio.2019.05.005
5. Zhou Y, Sharma N, Deshmukh P, Lakhman RK, Jain M, Kasi RM. Hierarchically structured free-standing hydrogels with liquid crystalline domains and magnetic nanoparticles as dual physical cross-linkers. J. Am. Chem. Soc. 2012;134(3):1630–1641. https://doi:10.1021/ja208349x
6. Xie W, Gao Q, Guo Z, Wang D, Gao F, Wang X, Wei Y, Zhao L. Injectable and self-healing thermosensitive magnetic hydrogel for asynchronous control release of doxorubicin and docetaxel to treat triple-negative breast cancer. ACS Appl. Mater. Interfaces 2017;9(39):33660–33673.
   DOI: 10.1021/acsami.7b10699
7. Noh M, Choi YH, An YH, Tahk D, Cho S, Yoon JW, Jeon NL, Park TH, Kim J, Hwang NS. Magnetic nanoparticle-embedded hydrogel sheet with a groove pattern for wound healing application. ACS Biomater. Sci. Eng. 2019;5(8):3909–3921. doi:10.1021/acsbiomaterials.8b01307
8. Tang J, Yin Q, Qiao Y, Wang T. Shape morphing of hydrogels in alternating magnetic field, ACS Appl. Mater. Interfaces. 2019);11(23):21194–21200. doi. org/10.1021/acsami.9b05742

9. Huang J, Liang Y, Huang Z, Zhao P, Liang Q, Liu Y, Duan L, Liu W, Zhu F, Bian L, Xia J, Xiong J, Wang D. Magnetic enhancement of chondrogenic differentiation of mesenchymal stem cells, ACS Biomater. Sci. Eng. 2019;5(5):2200–2207.
DOI: 10.1021/acsbiomaterials.9b00025
10. Huang J, Liang Y, Jia Z, Chen J, Duan L, Liu W, Zhu F, Liang Q, Zhu W, You W, Xiong J, Wang D. Development of magnetic nanocomposite hydrogel with potential cartilage tissue engineering. ACS Omega. 2018;3(6):6182–6189.
DOI: 10.1021/acsomega.8b00291
11. Zheng X, Wu D, Su T, Bao S, Liao C, Wang Q. Magnetic nanocomposite hydrogel prepared by ZnO-initiated photopolymerization for La (III) adsorption. ACS Appl. Mater. Interfaces. 2014;6(22):19840–19849.
DOI: 10.1021/am505177c
12. Tang SCN, Yan DYS, Lo IMC. Sustainable wastewater treatment using microsized magnetic hydrogel with magnetic separation technology. Ind. Eng. Chem. Res. 2014;53(40):15718–15724.
DOI: 10.1021/ie502512h
13. Czichy C, Spangenberg J, Günther S, Gelinsky M, Odenbach S. Determination of the Young's modulus for alginate-based hydrogel with magnetite-particles depending on storage conditions and particle concentration. J. Magn. Magn. Mater. 2020;501:166395.
DOI: 10.1016/j.jmmm.2020.166395
14. Xulu PM, Filipcsei G, Zrínyi M. Preparation and Responsive Properties of Magnetically Soft Poly(N-isopropylacrylamide) Gels. Macromolecules. 2000;33(5):1716–1719.
DOI: 10.1021/ma990967r
15. Filipcsei G, Csetneki I, Szilágyi A, Zrínyi M. Magnetic Field-Responsive Smart Polymer Composites. Advances in Polymer Science. 2007;206:137–189.
DOI: 10.1007/12_2006_104
16. Filipcsei G, Zrínyi M. Magnetodeformation Effects and the Swelling of Ferrogels in a Uniform Magnetic Field. J. Phys. Condens. 2010;22:276001.
DOI: 10.1088/0953–8984/22/27/276001
17. Galicia JA, Sandre O, Cousin F, Guemghar D, Menager C, Cabuil V. Designing magnetic composite materials using aqueous magnetic fluids. Journal of Physics: Condensed Matter. 2003;15(15):S1379 — S1402.
DOI: 10.1088/0953–8984/15/15/306
18. Galicia J A, Cousin F, Dubois E, Sandre O, Cabiul V and Perzynski R. Static and dynamic structural probing of swollen polyacrylamide ferrogels. Soft Matter. 2009;5(13):2614–2624.
DOI: 10.1039/b819189a
19. Galicia J A, Cousin F, Dubois E, Sandre O, Cabuil V and Perzynski R. Local structure of polymeric ferrogels. Journal of Magnetism and Magnetic Materials. 2011;323(10):1211–1215.
DOI: 10.1016/j.jmmm.2010.11.008

20. Shankar A, Safronov AP, Mikhnevich EA, Beketov IV. Multidomain iron nanoparticles for the preparation of polyacrylamide ferrogels. Journal of Magnetism and Magnetic Materials. 2017:431:134–137.
DOI: 10.1016/j.jmmm.2016.08.075
21. Shankar A, Safronov AP, Mikhnevich EA, Beketov IV, Kurlyandskaya GV. Ferrogels based on entrapped metallic iron nanoparticles in a polyacrylamide network: extended Derjaguin-Landau-Verwey-Overbeek consideration, interfacial interactions and magnetodeformation. Soft Matter. 2017;13(18):3359–3372.
DOI: 10.1039/C7SM00534B
22. Mikhnevich EA, Chebotkova PD, Safronov AP, Kurlyandskaya GV. Influence of uniform magnetic field on elastic modulus in polyacrylamide ferrogels with embedded nickel nanoparticles. Journal of Physics: Conference Series. 2019;1389(1):012059.
DOI: 10.1088/1742–6596/1389/1/012059
23. Kurlyandskaya GV, Safronov AP, Bhagat SM, Lofland SE, Beketov IV, Prieto ML. Tailoring functional properties of Ni nanoparticles-acrylic copolymer composites with different concentrations of magnetic filler. J. Appl. Phys. 2015;117:123917.
DOI: 10.1063/1.4916700
24. Beketov IV, Safronov AP, Medvedev AI, Murzakaev AM, Timoshenkova OR, Demina TM. In-situ formation of carbon shells on the surface of Ni nanoparticles synthesized by the electric explosion of wire. Nanosystems: physics, chemistry, mathematics. 2018;9(4):1–9.
DOI: 10.17586/2220-8054-2018-9-4-513-520
25. Beketov IV, Safronov AP, Bagazeev AV, Larrañaga A, Kurlyandskaya GV, Medvedev AI. In situ modification of Fe and Ni magnetic nanopowders produced by the electrical explosion of wire. Journal of Alloys and Compounds. 2014;586:S483 — S488.
DOI: 10.1016/j.jallcom.2013.01.152

Please note that all new submissions will be accepted in English only. Requirements for the manuscript preparation are available on the Journal's website and in the following template

Chimica Techno Acta manusctipt style guidelines (title)

A.N. Authorname[a], A.N. Authorname[b], A.N. Authorname[ab]

[a] Institution, address, city, country

[b] Institution, address, city, country

e-mail: corresponding_author@e-mail.com

Abstract

The abstract should be a single paragraph (up to 300 words) in plain text (that means — no formulae or references are permitted) that summarises the content of the article. It should set the main objectives and results of the work; giving the reader a clear idea of what has been achieved. An abstract should not be extremely short though — if yours is 1–2 sentences long, then you're not doing it right. Make sure that you use well-known, searchable terms and phrases.

Keywords: short; searchable; keywords (up to 10).

Introduction

An introduction should 'set the scene' of the work. It should clearly explain both the nature of the problem under investigation and its background. It should start off general and then focus in to the specific research question you are investigating. Ensure you include all relevant references.

Experimental (if appropiate)

Descriptions of the experiments should be provided in enough detail so that a skilled researcher is able to repeat them. Methods already published or experimental techniques already described elsewhere should be indicated by a reference. Only non-standard apparatus should be described in details; commercially available instruments are referred to by their stock numbers.

Results and discussion

This is undoubtedly the most important section of your article. It should consist of the logically ordered sequence of text, formulae, images and tables.

All formulae which appear in their own line should be numbered:

$$A = B + C \tag{1}$$

Tables should be used only when they can present information more efficiently than running text or even an image:

Table 1

Just an ordinary table without any sophisticated formatting applied

A	B	C	D
1	2	3	4
+	+	+	–

All illustrations should be of a high quality (300 dpi or higher) and should be placed in the flow of the text, not in the end of an article:

Fig. 1. Just an ordinary image

Please bear in mind that all illustrations and tables should fit smoothly within either single column (approx. 6 cm) or double column (approx. 12 cm) width.

Conclusions

Your conclusions should summarize the main paper, underline the interpretation of the key results and highlight the novelty and significance of the work. They may address some plans for relevant future work as well.

Acknowledgements (if appropiate)

All sources of funding such as grants should be declared here. Individuals who contributed to the research but are not co-authors may also be briefly acknowledged.

References

A reference should be indicated in square brackets in line with the text (e.g. [1]). The actual references in the reference list should be numbered in the order in which they appear in the text. In Chimica Techno Acta so-called Vancouver Citation Style is adopted almost as it is described in the following public domain textbook [1]:

1. Patrias K. Citing medicine: the NLM style guide for authors, editors, and publishers [Internet]. 2nd ed. Wendling DL, technical editor. Bethesda (MD): National Library of Medicine (US); 2007- [updated 2015 Oct 2; cited 2017 Jun 07]. Available from: http://www.nlm.nih.gov/citingmedicine

Note that opposed to [1] we omit the date of publication (leaving year only) of the referenced journal article, as almost all journals are continuously paginated throughout the volume. And another one — DOI or a hyperlink should always come last in a reference. These are the only major differences between our style and such described in [1], so when in doubt — you can always refer to [1], it contains tremendous number of well-organized examples.

For your convenience, below are some references to the different types of publications:

Books

2. Livingstone S. The Chemistry of Ruthenium, Rhodium, Palladium, Osmium, Iridium and Platinum. Oxford: Pergamon; 1973. 222 p.

3. Bard AJ, Faulkner LR. Electrochemical Methods: Fundamentals and Applications. 2nd ed. New York: John Wiley & Sons; 2001. 833 p.

Books not in English

4. Evdokimov AA, Efremov VA, Trunov VK, Kleyman IA, Tananaev IV. Soedineniya redkozemel'nykh elementov. Molibdaty, vol'framaty [Rare-earth elements' compounds. Molibdates, wolframates]. Moscow: Nauka; 1991. 267 p. Russian.

* Translation of the title in square brackets is not required, but highly desirable.

* For Cyrillic languages, such as Russian, please use consistent transliteration system. There are plenty, but we strongly recommend BGN/PCGN Romanization as it's one of the

easiest to read and implement (https://en.wikipedia.org/wiki/BGN/PCGN_romanization_of_Russian).

Journal articles

5. Zuev AYu, Tsvetkov DS. Oxygen nonstoichiometry, defect structure and defect-induced expansion of undoped perovskite $LaMnO_{3\pm\delta}$. Solid State Ionics. 2010;81(11–12):557–63. DOI:10.1016/j.ssi.2010.02.024

6. Shannon RD. Revised effective ionic radii and systematic studies of interatomic distances in halides and chalcogenides. Acta Cryst. 1976;A32:751–67. DOI:10.1107/S0567739476001551

7. Allred AL, Rochow EG. A scale of electronegativity based on electrostatic force. J Inorg Nucl Chem. 1958;5(4):264–8. DOI:10.1016/0022-1902(58)80003-2

* For the majority of chemical journals corresponding abbreviation is defined in Chemical Abstracts Service Source Index (CASSI, http://cassi.cas.org). If an abbreviation is not available there, please use the full name of a journal.

* Note that DOI of an article, when available, should always be provided.

Journal articles on the Internet (e.g. for online-only journals without DOI)

8. Tkach V, Nechyporuk V, Yagodynets P. Descripción matemática de la síntesis electroquímica de polímeros conductores en la presencia de surfactants. Avances en Química [Internet]. 2013[cited 2016];8(1):9–15. Spanish. Available from: http://erevistas.saber.ula.ve/index.php/avancesenquimica/article/download/6357/6168

Conference abstracts

9. Zuev AYu, Sereda VV, Malyshkin DA, Ivanov IL, Tsvetkov DS. Mechano-chemical coupling in double perovskites as energy related materials. In: Abstracts of the XX Mendeleev Congress on general and applied chemistry, Vol. 3; 2016 Sep 26–30; Ekaterinburg, Russia. p. 325.

10. Steparuk AS, Usachev SA, Tsvetkov DS, Sosnovskikh VYa, Zuev AYu. Novyy katodnyy material na osnove mayenita dlya elektrokhimicheskogo karboksilirovaniya organicheskikh soedineniy [New mayenite-based cathode material for electrochemical carboxylation of organic compounds]. In: Tezisy dokladov XXVI Rossiyskoy molodezhnoy nauchnoy konferentsii "Problemy teoreticheskoy i eksperimental'noy khimii" [Abstracts of XXVI Russian scientific conference for young scientists "Problems of theoretical and experimental chemistry"]; 2016 Apr 27–29; Ekaterinburg, Russia. p. 285–286. Russian.

Dissertations

11. ten Donkelaar SFP. Development of Stable Oxygen Transport Membranes [dissertation]. Enschede (The Netherlands): University of Twente; 2015. 140 p.

Patents

12. Chemezov OV, Batukhtin VP, Apisarov AP, Isakov AV, Zaikov YuP, inventors; Institute of High-Temperature Electrochemistry UB RAS, assignee. Sposob polucheniya nano- i mikrovolokon kremniya elektrolizom dioksida kremniya iz rasplavov soley. Russian Federation patent RU 2427526. 2011 Aug 27. Russian.

13. Menta E, Da Re G, Grugni M., authors; Cti Europe S.R.L., assignee. Derivatives of chromen-2-one as inhibitors of vegf production in mammalian cells. United States patent US20060122387 A1. 2006 Jun 8.

Chimica Techno Acta

Учредитель —
Уральский федеральный университет
имени первого Президента России Б. Н. Ельцина
620002, Россия, Екатеринбург, ул. Мира, 19

Свидетельство о регистрации
ПИ № ФС77-56173 от 15.11.2013

Адрес журнала:
Россия, 620000,
Екатеринбург, ул. Мира, 28, оф. Х-268
E-mail: t.a.pospelova@urfu.ru

Распространяется бесплатно.
Дата выхода в свет 07.10.2020. Формат 70×100/16.
Тираж 100 экз. Заказ № 167.

Отпечатано в типографии
Издательско-полиграфического центра УрФУ
620000, Екатеринбург, ул. Тургенева, 4
Тел.: +7 (343) 350-56-64, 350-90-13
Факс: +7 (343) 358-93-06
E-mail: press-urfu@mail.ru

Founded by Ural Federal University named after
the first President of Russia B. N. Yeltsin
19, Mira St., Ekaterinburg, 620002, Russia

Journal Registration Certificate
PI № FS 77-56173 as of 15.11.2013

Principal Contact
Office X-268, Mira Str.,
620000, Ekaterinburg, Russia
E-mail: t.a.pospelova@urfu.ru

Distributed for free.
Release date 07.10.2020. Format 70×100/16.
Circulation 100 cop.

Publisher — Ural Federal University
Publishing Centre
4, Turgenev St., 620000 Ekaterinburg, Russia
Phone: +7 343 350 56 64, +7 343 350 90 13
Fax: +7 343 358 93 06
E-mail: press-urfu@mail.ru